



Article

# Fluorescent Vitamin B<sub>12</sub>–Platinum(II) Derivatives as Potential Metallotheranostic Agents for the Treatment and Imaging of Tumors

Rozan Mehder <sup>1</sup>, Elena de la Torre-Rubio <sup>2,3</sup>, Isabel de la Cueva-Alique <sup>2</sup>, Ciaran O’Malley <sup>1,†</sup>, Adrián Pérez-Redondo <sup>2</sup> , Lourdes Gude <sup>2,3</sup> , Eva Royo <sup>2,3,\*</sup> and Luca Ronconi <sup>1,\*</sup>

<sup>1</sup> University of Galway, School of Biological and Chemical Sciences, H91 TK33 Galway, Ireland; r.mehder1@universityofgalway.ie (R.M.); ciaran.omalley@ul.ie (C.O.)

<sup>2</sup> Universidad de Alcalá, Departamento de Química Orgánica y Química Inorgánica, Instituto de Investigación Química “Andrés M. del Río” (IQAR), 28805 Alcalá de Henares, Spain; elena.torrer@uah.es (E.d.I.T.-R.); isabelcuevaalique@gmail.com (I.d.I.C.-A.); adrian.perez@uah.es (A.P.-R.); lourdes.gude@uah.es (L.G.)

<sup>3</sup> Design, Interaction and Synthesis of Bioactive Compounds (DISCOBAC) Research Group, Instituto de Investigación Sanitaria de Castilla-La Mancha (IDISCAM), 45071 Toledo, Spain

\* Correspondence: eva.royo@uah.es (E.R.); luca.ronconi@universityofgalway.ie (L.R.)

† Current address: University of Limerick, Department of Physics, Bernal Institute, V94 T9PX Limerick, Ireland.

**Abstract:** Vitamin B<sub>12</sub> (cyanocobalamin) is an essential nutrient with very low bioavailability. Compared with normal cells, tumor cells show an increased demand for vitamin B<sub>12</sub> to support their abnormal proliferation, which is a feature that can be exploited for the tumor-specific delivery of therapeutic and/or diagnostic agents by functionalizing vitamin B<sub>12</sub> with suitable metallodrugs and/or luminescent probes. In this context, we report on the design of fluorescent vitamin B<sub>12</sub>–metal conjugates of the type [FLUO–B<sub>12</sub>–{M}] in which cyanocobalamin is functionalized at the 5'-site of the ribose unit with a fluorophore (FLUO: rhodamine 6G), whereas the Co(III)-cyano moiety is *N*-coordinated to a metal-based anticancer scaffold (*{M}*: Pt(II) substrate bearing enantiopure phenylamino-oxime ligands derived from *R*- or *S*-limonene). Two novel fluorescent cyanocobalamin–platinum(II) derivatives and their corresponding non-fluorescent counterparts were successfully generated and fully characterized, including the evaluation of their lipophilicity and luminescent properties. Although they exhibit low antiproliferative activity ( $IC_{50} = 40\text{--}70 \mu\text{M}$ ), both fluorescent vitamin B<sub>12</sub>–platinum(II) conjugates showed an enhanced capability to inhibit cell viability compared with the inactive metal precursors and the non-fluorescent vitamin B<sub>12</sub>–platinum(II) analogues, confirming the beneficial effect of functionalization with the rhodamine 6G scaffold not only for imaging purposes but also with the aim of improving their biological activity.

**Keywords:** vitamin B<sub>12</sub>; platinum complexes; rhodamine 6G; metallodrugs; anticancer drugs; tumor imaging; fluorescence



**Citation:** Mehder, R.; de la Torre-Rubio, E.; de la Cueva-Alique, I.; O’Malley, C.; Pérez-Redondo, A.; Gude, L.; Royo, E.; Ronconi, L. Fluorescent Vitamin B<sub>12</sub>–Platinum(II) Derivatives as Potential Metallotheranostic Agents for the Treatment and Imaging of Tumors. *Inorganics* **2024**, *12*, 91. <https://doi.org/10.3390/inorganics12030091>

Academic Editors: Yong Wang and Kang-Nan Wang

Received: 19 February 2024

Revised: 12 March 2024

Accepted: 13 March 2024

Published: 21 March 2024



**Copyright:** © 2024 by the authors. Licensee MDPI, Basel, Switzerland. This article is an open access article distributed under the terms and conditions of the Creative Commons Attribution (CC BY) license (<https://creativecommons.org/licenses/by/4.0/>).

## 1. Introduction

Although still largely exploited in cancer treatment, conventional chemotherapy based on broad-spectrum cytotoxic chemotherapeutics presents several drawbacks arising from its general incapability to selectively target tumor cells over normal ones, often resulting in the onset of severe side effects associated with its toxicity [1]. In this context, clinically established platinum drugs (i.e., cisplatin, carboplatin, and oxaliplatin) are no exception: in fact, despite their undebatable therapeutic efficacy for the treatment of many types of tumors, their lack of specificity often induces systemic toxicity besides killing cancer cells [2]. Therefore, the rational design of tumor-selective drugs has been a major research priority during the past two decades [3], especially since the approval of the first small-molecule targeted drug, imatinib (a tyrosine kinase inhibitor), in 2002 for clinical use for the treatment of gastrointestinal stromal tumors and leukemia [4]. Recent advances in the

understanding of the multistep development of tumors have led to the identification of well-defined hallmarks shared by most (possibly all) types of malignancies [5]. Accordingly, focusing on one or more of such hallmark capabilities of tumor cells would support the development of tumor-selective drugs. The fundamental concept of so-called targeted chemotherapy relies on the ideal assumption that a chemotherapeutic drug should be delivered and accumulate selectively at the tumor site but not in the rest of the body. Therefore, the conjugation of a bioactive drug to a tumor-targeting (bio)molecule would generate a “smart bomb” for cancer treatment [6].

Amongst the many potential options available, vitamin B<sub>12</sub> may be used as a carrier to achieve the tumor-selective delivery of drugs [7,8]. Vitamin B<sub>12</sub> (B<sub>12</sub>, first isolated as cyanocobalamin (Figure 1)) is an essential micronutrient of microbial origin. The recommended daily intake for adults is 2.5 µg, and since it is not produced within the human body, it must be sourced from animal-derived foods or supplements [9]. The metabolism of vitamin B<sub>12</sub> in humans is rather complex and involves the action of three transport proteins, namely haptocorrin (also known as transcobalamin I), gastric intrinsic factor, and transcobalamin II, which support its transport from the oral cavity to the cells. Once released into the cytoplasm, free vitamin B<sub>12</sub> is converted into its biologically active forms: methylcobalamin (a coenzyme necessary for the methylation of homocysteine) and 5'-deoxyadenosylcobalamin (acting as a cofactor to convert methylmalonyl-coenzymeA into succinyl-coenzyme A, which subsequently enters the Krebs cycle to produce energy) [10]. Consequently, the fact that rapidly dividing tumor cells, requiring higher amounts of methionine and energy to sustain their abnormal growth, show a preferential accumulation of cyanocobalamin compared with healthy cells is not at all surprising. Such increased demand of vitamin B<sub>12</sub> by cancer cells makes it very attractive to selectively target tumor sites [11].

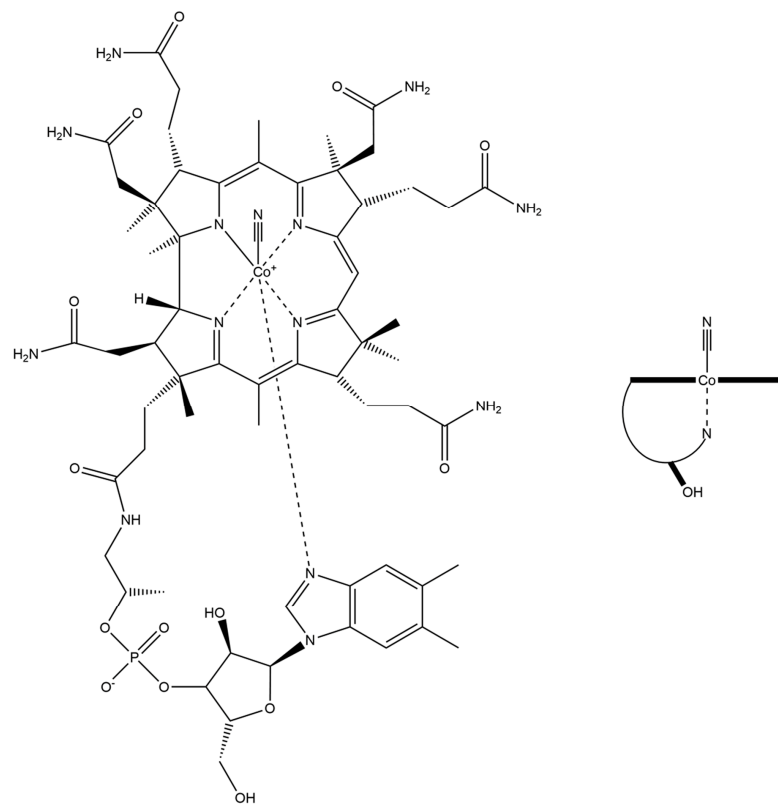


**Figure 1.** Structure (left) and schematic representation (right) of vitamin B<sub>12</sub> (cyanocobalamin).

Positive outcomes were reported by Alberto and coworkers for some vitamin B<sub>12</sub>–platinum(II) conjugates in which cisplatin-like derivatives are bound to the cyano group of

the vitamin [12–15]. Such conjugates were shown to be taken up preferentially by cancer cells at higher amounts compared with native vitamin B<sub>12</sub>, thus providing a promising proof of concept supporting the rationale of the proposed strategy [16]. A similar approach was successfully used to design cyanocobalamin-functionalized technetium-based radiopharmaceuticals [17] and ruthenium(II)-based anticancer agents [18]. Finally, it was recently reported that vitamin B<sub>12</sub> exhibited synergistic anticancer effects in combination therapy towards different tumor cell lines, suggesting its use as a potential adjunctive treatment option for some cancer types [19].

On account of the aforementioned considerations, such avidity of cyanocobalamin in cancers may be exploited for the site-specific delivery of drugs directly into the tumor by conjugating vitamin B<sub>12</sub> (carrier) to either anticancer (chemotherapeutics) or imaging (fluorophores) agents. In particular, vitamin B<sub>12</sub> derivatives functionalized with suitable fluorophores can be conjugated to metal-based chemotherapeutics so as to attain the site-specific delivery of drugs into the affected tissues [20–22]. Accordingly, with reference to Figure 2, our aim was to design fluorescent vitamin B<sub>12</sub>–metal conjugates of the type [FLUO–B<sub>12</sub>–{M}] in which cyanocobalamin is functionalized at the 5'-hydroxo group of the ribose unit with a fluorophore (FLUO: rhodamine 6G), whereas the Co(III)–cyano moiety is coordinated to a metal-based scaffold ({M}: Pt(II) substrate bearing enantiopure phenylamino-oxime ligands derived from *R*- or *S*-limonene). The rationale behind the proposed designing approach is based on the evidence that vitamin B<sub>12</sub> is converted into its cofactors (methylcobalamin and adenosylcobalamin) inside the cell upon reduction of Co(III) to Co(II), followed by the subsequent release of the cyano group. Therefore, by binding metal-containing bioactive substrates to the cyanocobalamin Co(III)–CN moiety, should the overall bioconjugate accumulate preferentially in the tumor cells, the potentially cytotoxic species {CN–metallodrug} would be expected to be released directly into the diseased site where it could exert its anticancer activity without affecting healthy tissues. Additionally, the fluorophore attached at the 5'-ribose moiety would allow the transport and biodistribution to be followed and assessed by fluorescence spectroscopy [12,13,17]. Therefore, the goal is to take advantage of the increased demand for cyanocobalamin in tumor cells by exploiting its carrier properties to design selective “Trojan Horse”-type theranostics in which the structural features of vitamin B<sub>12</sub> conceal both the attached imaging agent and the metallodrug so as to achieve a better therapeutic outcome and reduce side effects. Potentially, this designing strategy has a two-fold advantage: (i) to combine the anticancer properties of metal derivatives with the tumor-targeting properties provided by the coordinated cyanocobalamin and (ii) to exploit the conjugated fluorescent probe for tumor imaging.

Specifically, two novel fluorescent cyanocobalamin–platinum(II) derivatives and their corresponding non-fluorescent counterparts were successfully generated and fully characterized, and their lipophilicity and luminescent properties were evaluated. Preliminary in vitro biological studies, such as antiproliferative activity, cell uptake, and the effect on the cell cycle, were also carried out, together with the evaluation of metal conjugate–DNA interactions. The results are discussed in relation to the data available in the literature to date.

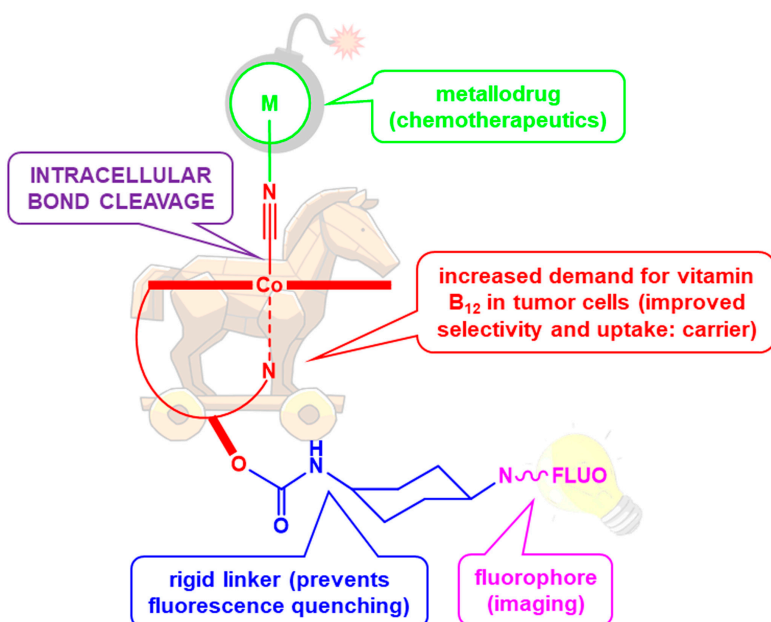


**Figure 2.** General design of the target fluorescent vitamin B<sub>12</sub>–metallodrug conjugates [FLUO–B<sub>12</sub>–{M}] reported here (FLUO = fluorophore; {M} = metal-based scaffold).

## 2. Results and Discussion

### 2.1. Syntheses and Characterizations

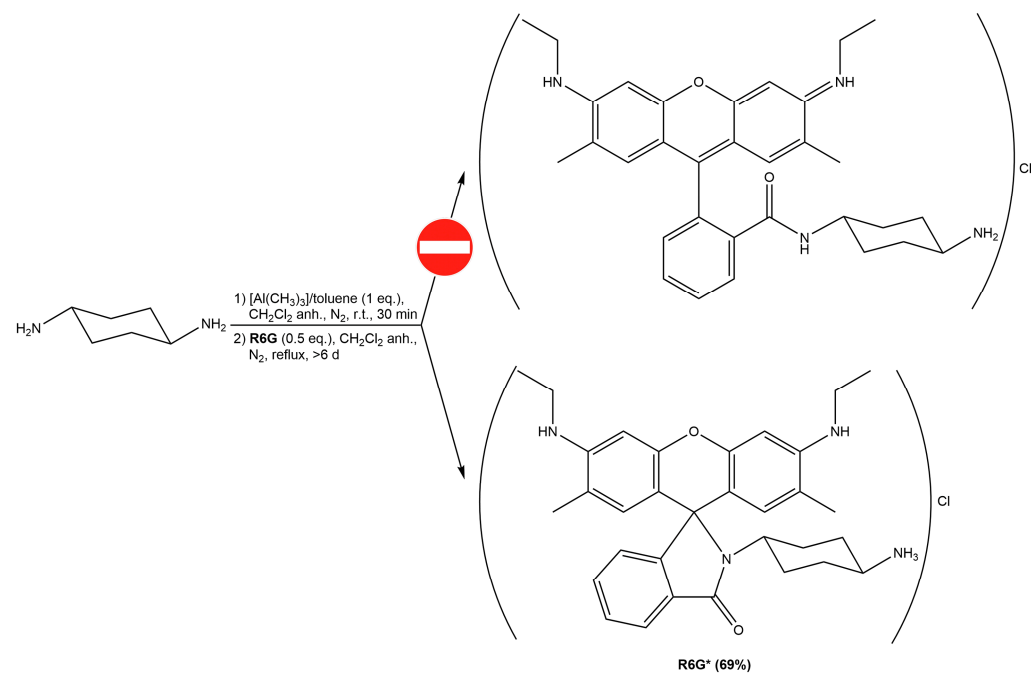
All intermediates and newly synthesized species were purified by HPLC and characterized by MS, FT-IR, and mono- and multidimensional NMR spectroscopy. The detailed synthetic procedures and spectroscopic data are reported in the Supplementary Materials.

#### 2.1.1. Fluorophore-Functionalized Cyanocobalamin

In order to preserve the biological functionality of vitamin B<sub>12</sub>, chemical modifications should not impair the interaction with the transport proteins required for intracellular trafficking and endocytosis. In this regard, the 5'-hydroxo group of the ribose unit proved to be the most favorable site for attaching large molecules without affecting the recognition of vitamin B<sub>12</sub> by such proteins, thus allowing it to be recognized, transported, and internalized inside the cell [23–27]. Accordingly, the first phase involved the functionalization of the 5'-site of the ribose with a suitable fluorophore through a spacer. Specifically, the rigid linker *trans*-1,4-diaminocyclohexane was incorporated with the aim of orienting the fluorophore afar from the corrin ring of cyanocobalamin in order to minimize intramolecular dynamic interactions with vitamin B<sub>12</sub> that would impair the luminescent properties of the fluorophore [28].

Vitamin B<sub>12</sub> was successfully functionalized at the 5'-site of the ribose moiety with the commercially available fluorophore rhodamine 6G (**R6G**). This multi-step synthesis was initially carried out following a literature procedure [28], which proved to be somewhat inefficient in terms of yield and purity and, as such, required the implementation of a number of modifications to the experimental procedure. The first step (Scheme 1) involved the replacement of the ethyl ester of **R6G** with the rigid linker *trans*-1,4-diaminocyclohexane through the formation of an amide bond in the presence of Al(CH<sub>3</sub>)<sub>3</sub>. In contrast to what was previously reported, the final purified species **R6G\*** did not fully preserve the original structure of rhodamine 6G. Rhodamine-based dyes are well known to undergo structural interconversion in solution. For example, rhodamine 10 (that is, the non-esterified precursor of rhodamine 6G) may exist at the equilibrium in different structural isomers (namely native, zwitterion, and lactone forms) depending on the experimental conditions [29]. In our specific case, the formation of lactam form was confirmed by X-ray crystallography

(Figure 3), which is consistent with the molecular structure reported for other similar functionalized lactam-type rhodamine 6G derivatives [30,31].



**Scheme 1.** Synthesis of *trans*-1,4-diaminocyclohexane-functionalized rhodamine 6G (**R6G\***).

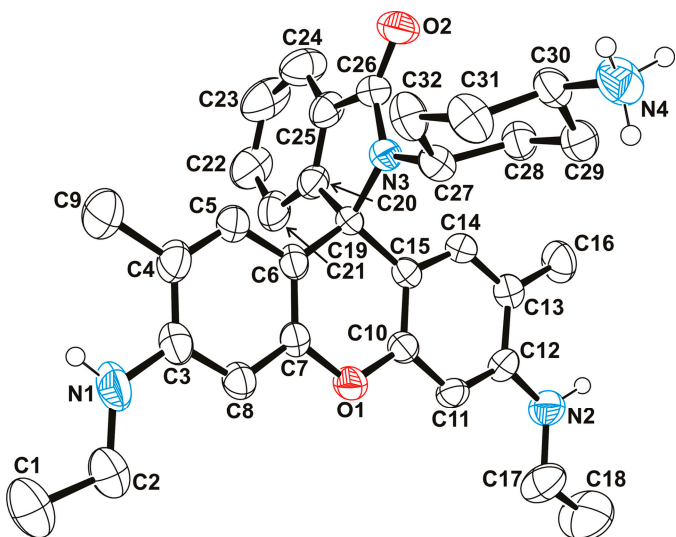
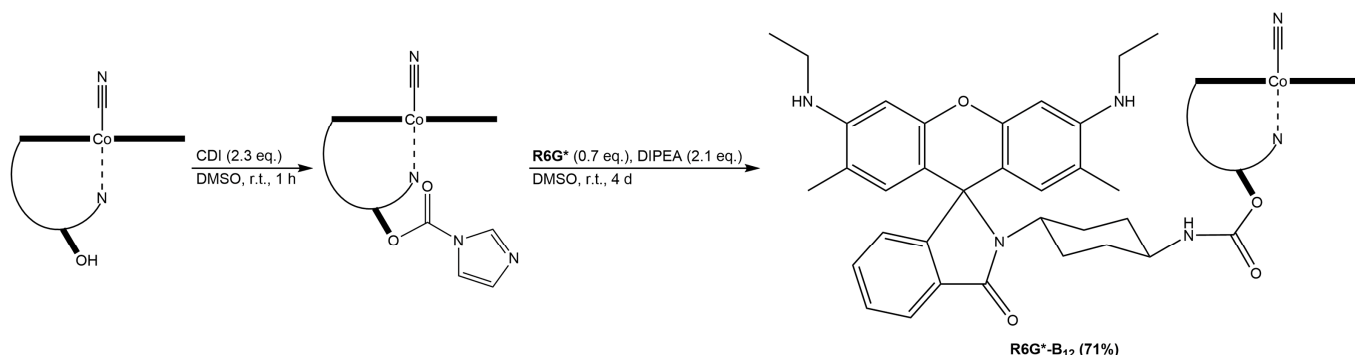


**Figure 3.** Molecular structure with atom numbering scheme of *trans*-1,4-diaminocyclohexane-functionalized rhodamine 6G precursor (**R6G\***, CCDC 2321413). Thermal ellipsoids are depicted at 50% probability level, and hydrogen atoms bonded to carbon atoms are omitted for clarity (see Supplementary Materials for details).

From a spectroscopic point of view, this was also supported by the disappearance in the IR spectrum of **R6G\*** of the vibrations at 3636, 1648, and 1566 cm<sup>-1</sup> assigned to  $\nu(\text{NH})$ ,  $\nu(\text{C}=\text{N})$ , and  $\delta(\text{C}=\text{N}-\text{H})$ , respectively, of the “iminium” group recorded for the starting reagent **R6G**, together with the recording of new bands at ~2900 ( $\nu_{\text{a,s}}$ ), 1622 ( $\delta_a$ ), and 1518 ( $\delta_s$ ) cm<sup>-1</sup> associated with the protonated NH<sub>3</sub><sup>+</sup> of the cyclohexyl pendant [29,32].

The second step led to the generation of the fluorescent vitamin B<sub>12</sub> intermediate **R6G\*-B<sub>12</sub>** (Scheme 2). In contrast to what was reported in reference [28], 1,1'-carbonyldiimidazole

(CDI) proved to be much more efficient than 1,1'-carbonyl-di-(1,2,4-triazole) as an acylating agent for the activation of the 5'-hydroxide group of the ribose moiety of cyanocobalamin. The coupling of the fluorescent probe was then achieved upon the nucleophilic attack of the amino group of rhodamine 6G-*trans*-1,4-diaminocyclohexane (**R6G\***) through the inclusion of a carbamate linkage, yielding the desired adduct **R6G\*-B<sub>12</sub>** in a 71% yield after column chromatography purification.



**Scheme 2.** Synthesis of the fluorescent vitamin B<sub>12</sub> intermediate **R6G\*-B<sub>12</sub>**.

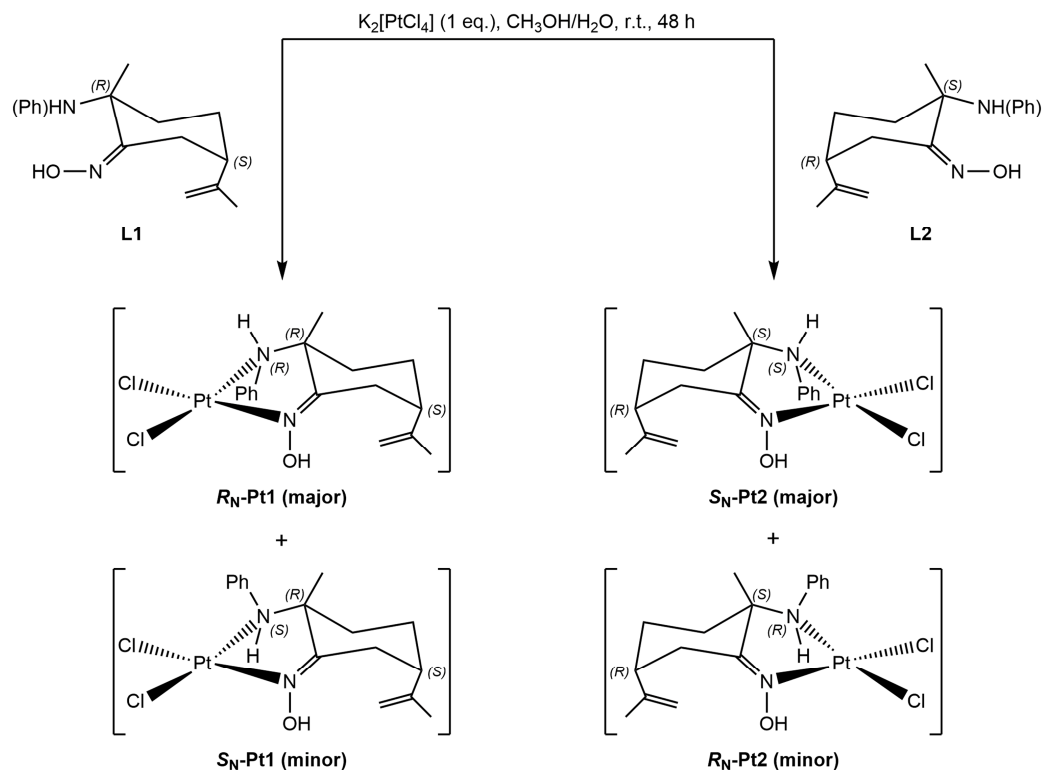
The composition of the final compound was confirmed by HRMS, which returned peaks for  $[M + H]^+$ ,  $[M + 2H]^{2+}$ , and  $[M + 3H]^{3+}$  at 1892.9083 (calcd. 1892.8564), 946.9586 (calcd. 946.9319), and 631.6422 (calcd. 631.6237)  $m/z$ , respectively, in agreement with the data reported in the literature [28]. As expected, the IR and NMR spectra of **R6G\*-B<sub>12</sub>** appeared like superimpositions of the individual IR and NMR spectra of vitamin B<sub>12</sub> and **R6G\***. The only notable difference was the appearance of a new signal at 177.4 ppm in the  $^{13}\text{C}^{\{1\}\text{H}}$  NMR spectrum of **R6G\*-B<sub>12</sub>** (absent in the spectra of both the **R6G\*** and vitamin B<sub>12</sub> precursors) assigned to the carbamate C=O group, as well as a general downfield shift of the  $^1\text{H}$  and  $^{13}\text{C}$  chemical shifts of the groups which were most directly affected by the formation of the linkage between the ribose moiety of cyanocobalamin ( $\text{C}^{\text{R}5}\text{H}_2$ : from 3.75–3.92 to 4.07–4.11 ppm;  $\text{C}^{\text{R}5}\text{H}_2$ : from 62.7 to 64.0 ppm) and the *trans*-1,4-diamidocyclohexane linker of **R6G\*** ( $\text{C}^{\text{a}4}\text{H}$ : from 2.93 to 3.27 ppm;  $\text{C}^{\text{a}4}\text{H}$ : from 49.7 to 50.4 ppm).

### 2.1.2. Amino-Oxime Platinum(II) Complexes

Stereochemistry is well known to play a major role in the activity of biologically active species [33], and the anticancer properties of some chiral platinum derivatives have been reported [34]. In this context, natural terpenes are enantiomerically pure, commercially available low-cost reagents that may be used as building blocks to prepare optically active metal derivatives through the exploitation of known stereoselective functionalization procedures [35]. Royo and coworkers previously reported on the use of chiral amino-oxime organic compounds derived from *R*- and *S*-limonene to prepare water-soluble, enantiopure Ru(II) [36,37], Ti(IV) [38,39], Pd(II) [40], and Pt(II) [41] derivatives with relevant antitumor properties. The rationale behind the aforementioned designing strategy relies on the fact that both amino and oxime functional groups are versatile building blocks for the design of soluble and stable metal compounds under physiological conditions [42,43]. Additionally, the derivatization of organic scaffolds with oxime groups has shown interesting biological properties, such as the inhibition of several protein kinases, as well as anti-inflammatory, analgesic, bactericidal, antiviral, and anticancer activities [44].

In this regard, given our interest in the use of enantiopure phenylamino-oxime proligands derived from limonene to design new metal-based agents with potential anticancer effects, the (2*R*,5*S*)-2-methyl-5-(1-methylethenyl)-2-(phenylamino)-cyclohexanone oxime (**L1**) ligand and the corresponding (2*S*,5*R*)-2-methyl-5-(1-methylethenyl)-2-(phenylamino)-cyclohexanone oxime (**L2**) enantiomer were synthesized as previously described [45] and subsequently coordinated to Pt(II) centers. With reference to Scheme 3, equimolar amounts

of  $K_2[PtCl_4]$  and either **L1** or **L2** were reacted in a  $H_2O/MeOH$  mixture, yielding the corresponding platinum(II) derivatives **Pt1** and **Pt2**, respectively.



**Scheme 3.** Synthesis of amino-oxime platinum(II) complexes  $R_N\text{-}/S_N\text{-Pt}1$  and  $S_N\text{-}/R_N\text{-Pt}2$ .

Interestingly, both platinum(II) complexes were obtained as a mixture of  $R_N$  and  $S_N$  epimers of the title compounds consequently to the  $N$ -donor of the amine function of the ligands becoming chiral upon coordination. This is evident, for example, in the  $^1H$  NMR spectrum of **Pt1**, where all hydrogen signals were assigned with the aid of  $[^{1H}, ^1H]$  COSY,  $^{13}C[^1H]$  NMR,  $^{13}C[^1H]$  DEPT, and  $[^1H, ^{13}C]$  HMQC experiments (see Supplementary Materials for details). An  $R_N\text{-Pt}1:S_N\text{-Pt}1$  epimers ratio of ca. 2.5:1 was estimated by  $^1H$  NMR in  $CD_3OD$ , where the mixture remained unchanged over 72 h.

The pure major epimer  $R_N\text{-Pt}1$  could be isolated by recrystallization from chloroform (89% yield). However, upon dissolution in various solvents, an epimerization process involving the coordinated amino moiety occurred [40,46,47], again leading to a final  $R_N\text{-Pt}1:S_N\text{-Pt}1$  ratio of ca. 2.5:1 in both  $CDCl_3$  (within 24 h) and  $CD_3OD$  (within a few minutes), as estimated by  $^1H$  NMR spectroscopy. Eventually, a full NMR characterization of each epimer was carried out in  $CDCl_3$ , in which solvent (unlike  $CD_3OD$ ) the  $^1H$  peaks of the oxime ( $\text{C=NOH}$ ) and amino ( $\text{C-N(Ph)H}$ ) moieties could be detected, thus allowing the carrying out of  $[^1H, ^{13}C]$  and  $[^1H, ^{15}N]$  HMBC experiments. The chemical shift changes of the  $^{15}N$  signals arising from the oxime and amino groups of **Pt1** (at 247.6 and 51.2 ppm, respectively, for  $R_N\text{-Pt}1$ ,  $^{15}N$  resonances of the minor epimer  $S_N\text{-Pt}1$  could not be detected) compared with the free ligand **L1** (at 343.5 and 84.1 ppm, respectively) are consistent with a  $\kappa^2N$ -bidentate coordination of the ligand to the metal center. In addition, the  $^{13}C$  resonances due to the  $\text{C=NOH}$  and  $\text{C-N(Ph)H}$  groups ( $R_N\text{-Pt}1$ : 171.6 and 75.7 ppm;  $S_N\text{-Pt}1$ : 170.6 and 75.1 ppm) showed a marked downfield shift relative to the same peaks found for **L1** (164.9 and 57.0 ppm). Epimerization was also evaluated in both solvents at increasing temperatures (up to 70 °C), which did not significantly affect the final ratio of the  $R_N\text{-Pt}1$  and  $S_N\text{-Pt}1$  epimers in the solution with respect to room temperature.

IR spectroscopy proved to be useful to further confirm the successful generation of the platinum(II) complex. The most diagnostic bands were assigned to vibrations

involving the groups directly coordinated to the metal center, that is, the oxime and amino nitrogen donors. For instance,  $\nu(\text{OH})_{\text{oxime}}$  ( $3307 \text{ cm}^{-1}$ ) and  $\nu(\text{NH})_{\text{amine}}$  ( $3205 \text{ cm}^{-1}$ ) appear much sharper and resolved than in the free ligand, as reported in the literature [40], and  $\nu(\text{C}=\text{N})_{\text{oxime}}$ ,  $\nu(\text{Ph}-\text{N})_{\text{amine}}$ , and  $\nu(\text{N}-\text{OH})_{\text{oxime}}$  (at  $1599$ ,  $1236$ , and  $910 \text{ cm}^{-1}$ , respectively) show a general shift to lower wavenumbers upon metal binding, which is in agreement with the data in the literature [48,49]. Additional information was obtained from the far-IR spectrum of **Pt1** (Figure 4). With respect to the free ligand **L1**, two new intense bands were recorded at  $350$  and  $336$ – $327 \text{ cm}^{-1}$ , assigned to  $\nu(\text{Pt}-\text{NPh})$  [49] and  $\nu(\text{Cl}-\text{Pt}-\text{Cl})$  [50], respectively. The  $\nu(\text{Pt}-\text{NOH})$  vibration was tentatively assigned to the band at  $451 \text{ cm}^{-1}$  based on the only associated data retrieved from the literature [48].

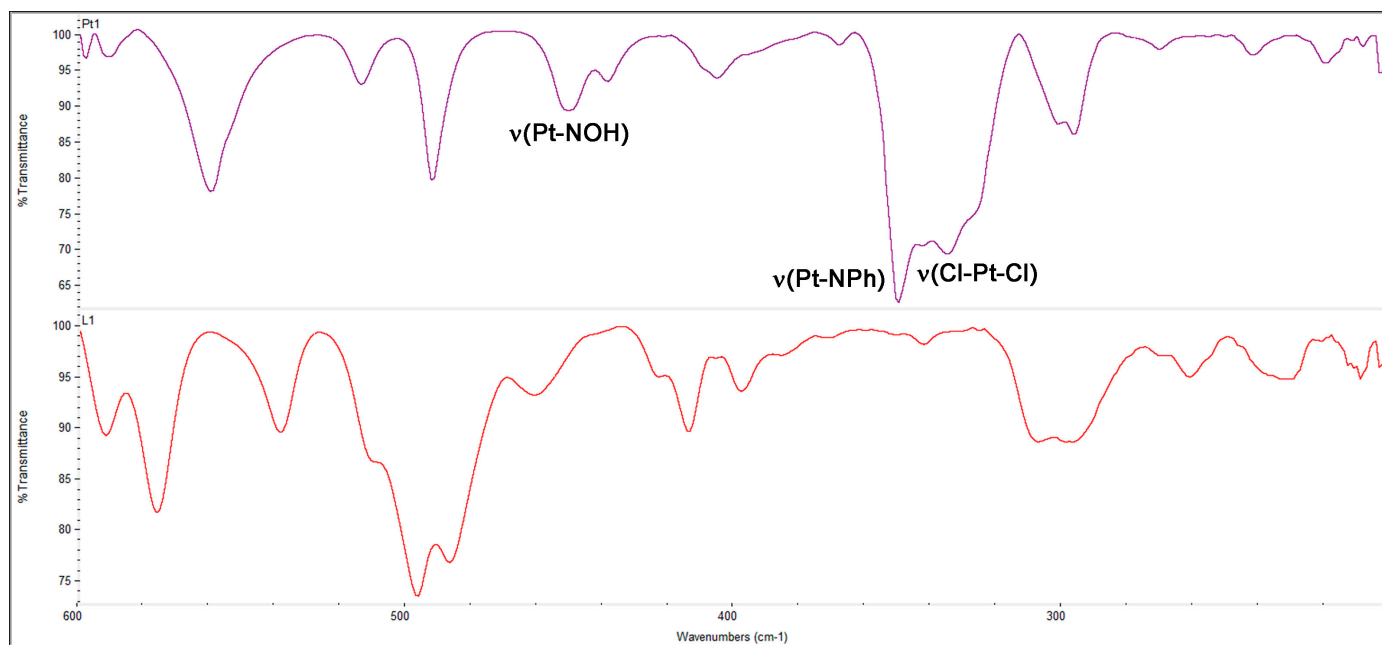


**Figure 4.** Comparison of the far-IR spectra in CsI of the platinum(II) complex **Pt1** (top) and the free ligand **L1** (bottom).

Crystals suitable for X-ray crystallography were obtained for **R<sub>N</sub>-Pt1**. With reference to Figure 5, the platinum(II) center shows a square planar geometry resulting from the bidentate coordination of the **L1** ligand through the oxime and amino nitrogen donor atoms, with the remaining coordination sites being occupied by two chlorido ligands. The crystal structure also confirmed the absolute configuration of the complex, namely *R<sub>N</sub>,2*R*,5*S**. The most characteristic feature of the molecule is the short intramolecular =N—O—H···Cl—Pt contact, with a O(1)···Cl(1) distance of  $3.12(1)$  Å [40,41,51].

Identical results were observed for the second platinum(II) complex **Pt2**, which was also obtained as a ca. 2.5:1 epimers ratio mixture of **S<sub>N</sub>-Pt2** and **R<sub>N</sub>-Pt2**, respectively, as estimated by <sup>1</sup>H NMR. Although the pure major epimer **S<sub>N</sub>-Pt2** could also be isolated by recrystallization from chloroform (94% yield), unfortunately, no crystals suitable for X-ray crystallography were obtained. Nevertheless, a comparison of the IR and NMR spectra of **Pt2** and **Pt1** confirmed their enantiomeric relationship (see Supplementary Materials for details).

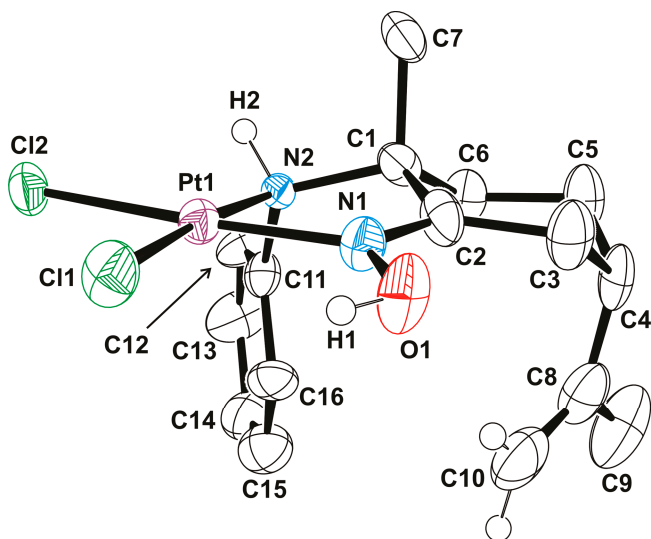


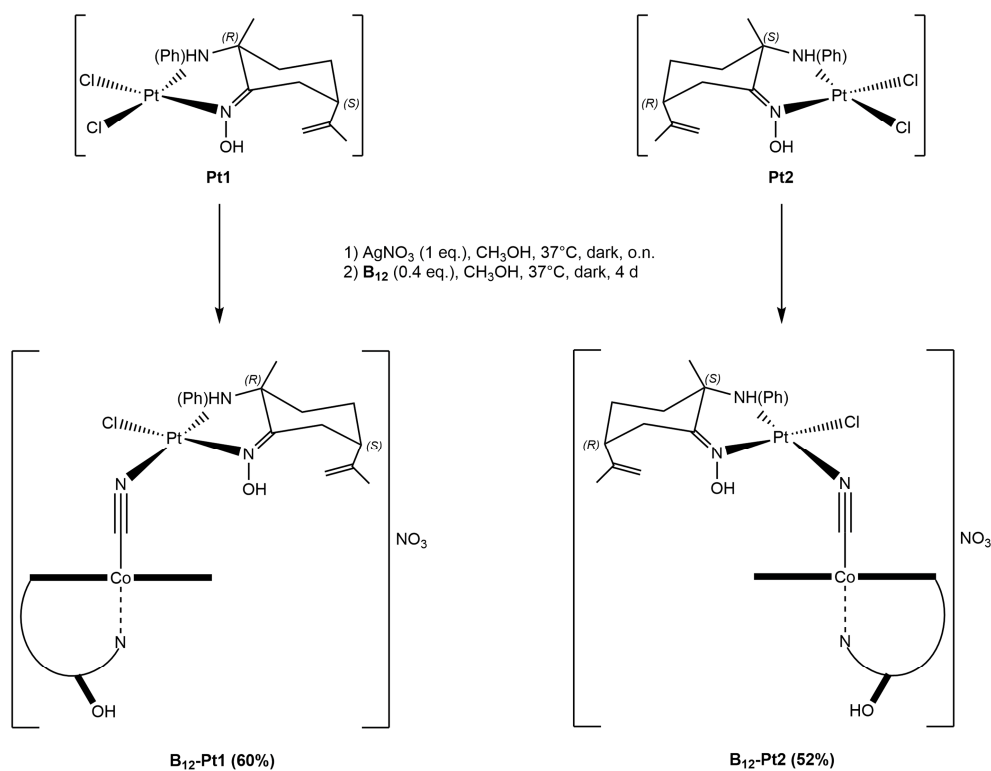
**Figure 5.** Molecular structure with atom numbering scheme of  $R_N\text{-Pt1}$  (CCDC 2321414). Thermal ellipsoids are depicted at 50% probability level, and hydrogen atoms bonded to carbon atoms are omitted for clarity (see Supplementary Materials for details).

### 2.1.3. Vitamin B<sub>12</sub>–Platinum(II) Derivatives

Prior to generating the target fluorescent vitamin B<sub>12</sub>–platinum(II) derivatives, we first focused on testing and optimizing the synthetic protocol by synthesizing the model non-fluorescent metal conjugates. As shown in Scheme 4, the metal precursor (either Pt1 or Pt2) was first treated with 1 eq. of AgNO<sub>3</sub> in order to remove one chloride, thus leading to the corresponding aquo intermediate. AgCl was then filtered off, and the resulting filtrate was reacted with 0.4 eq. of vitamin B<sub>12</sub> at 37 °C in the dark for four days. Such experimental conditions were dictated by the fact that in the Co<sup>III</sup>–CN moiety, the lone pair located on the nitrogen atom is strongly attracted towards the metal center in the +3 oxidation state, which makes it less available to further coordinate another metal center in a bridging mode. Therefore, an excess of platinum(II) precursors and long reaction times were chosen in order to “push” the reaction towards the desired product given the fact that higher temperatures cannot be used to prevent the thermal degradation of cyanocobalamin.

After evaporating the solvent, the crude product was purified by semi-preparative reversed-phase HPLC, yielding the expected vitamin B<sub>12</sub>–platinum(II) conjugates in moderate to good yields (**B**<sub>12</sub>–Pt1: 60%; **B**<sub>12</sub>–Pt2: 52%). The composition of the final compounds was confirmed by HRMS, which returned the peaks of [M–NO<sub>3</sub>]<sup>+</sup> (calcd. 1843.6750  $m/z$ ) and [M–NO<sub>3</sub> + H]<sup>2+</sup> (calcd. 922.3411  $m/z$ ) at 1843.6679/922.3399  $m/z$  and 1843.6763/922.3437  $m/z$  for **B**<sub>12</sub>–Pt1 and **B**<sub>12</sub>–Pt2, respectively.

As previously discussed, the starting platinum(II) complex Pt1 was actually a ca. 2.5:1 mixture of **R**<sub>N</sub>–Pt1 and **S**<sub>N</sub>–Pt1 epimers. Upon reaction with vitamin B<sub>12</sub>, indeed, some NMR signals assignable to two different stereoisomers (namely **B**<sub>12</sub>–(*R*<sub>N</sub>)–Pt1 and **B**<sub>12</sub>–(*S*<sub>N</sub>)–Pt1) were observed, and a ratio of ca. 2.1:1 in CD<sub>3</sub>OD could be estimated by <sup>1</sup>H NMR spectroscopy. However, the elucidation of the absolute configuration around the chiral amino nitrogen atom could not be achieved in solution due to the complexity of the NMR spectra and the major overlapping of the signals. Analogous results were obtained for the vitamin B<sub>12</sub>–platinum(II) conjugate **B**<sub>12</sub>–Pt2, for which a **B**<sub>12</sub>–(*S*<sub>N</sub>)–Pt2:**B**<sub>12</sub>–(*R*<sub>N</sub>)–Pt2 ratio of ca. 2.5:1 was also detected.



**Scheme 4.** Synthesis of non-fluorescent vitamin  $\text{B}_{12}$ –platinum(II) complexes  **$\text{B}_{12}\text{-Pt1}$**  and  **$\text{B}_{12}\text{-Pt2}$** .

A detailed analysis of the  $^1\text{H}$  NMR,  $[^1\text{H}, ^1\text{H}]$  COSY,  $^{13}\text{C}\{^1\text{H}\}$  NMR, and  $[^1\text{H}, ^{13}\text{C}]$  HSQC spectra of the cyanocobalamin–metal conjugates supported the proposed structures (see Supplementary Materials for details). Overall, the NMR spectra of both  **$\text{B}_{12}\text{-Pt1}$**  and  **$\text{B}_{12}\text{-Pt2}$**  appeared as superimpositions of the spectra of the starting reagents vitamin  $\text{B}_{12}$  and **Pt1/Pt2**, with the only significant changes being observed for the  $^{13}\text{C}$  signals of the groups in the closest proximity of the newly formed  $\text{CoCN}$ –Pt bond. For example, with reference to Figure 6, showing a comparison of the  $^{13}\text{C}\{^1\text{H}\}$  NMR spectra of cyanocobalamin, **Pt1** and the corresponding conjugate  **$\text{B}_{12}\text{-Pt1}$**  in the range of 40–190 ppm, the major chemical shift changes were recorded for  $\text{C}^{1\text{Pt}}$  (from 171.6 to 178.0 ppm) and  $\text{C}^{2\text{Pt}}$  (from 75.1 to 76.4 ppm) of the carbon atoms of the amino-oxime ligand directly attached to the nitrogen donors coordinated to the platinum(II) ion, which reflect a change in the coordination sphere around the platinum(II) center. Remarkably, the major shift was recorded for the CN peak, which moved downfield from 112.4 ppm in the free cyanocobalamin to 124.3 ppm in the corresponding platinum(II) conjugate, which is consistent with the presence of a bridged cyano moiety between the Co(III) and Pt(II) centers [52,53]. All of the other  $^{13}\text{C}$  peaks remained substantially unchanged, with the exception of a small downfield shift (approximately 1 ppm) for the  $\text{C}^{26}\text{H}_2$ ,  $\text{C}^1$ , and  $\text{C}^4$  signals of vitamin  $\text{B}_{12}$ . Remarkably, such groups all belong to the top-left quadrant of the corrin ring of cyanocobalamin, suggesting some sort of spatial proximity of the amino-oxime scaffold of the platinum(II) complex to that specific area of vitamin  $\text{B}_{12}$ , although this could only be confirmed through an X-ray structure. Interestingly, in the  $^{31}\text{P}\{^1\text{H}\}$  NMR spectra, only one peak at  $-0.1$  ( **$\text{B}_{12}\text{-Pt1}$** )/ $-0.2$  ( **$\text{B}_{12}\text{-Pt2}$** ) ppm (assigned to the phosphate group of vitamin  $\text{B}_{12}$  and normally found at 0.3 ppm for the starting cyanocobalamin) was recorded, indicating that the presence of either platinum(II) epimer would not affect the  $^{31}\text{P}$  resonances.

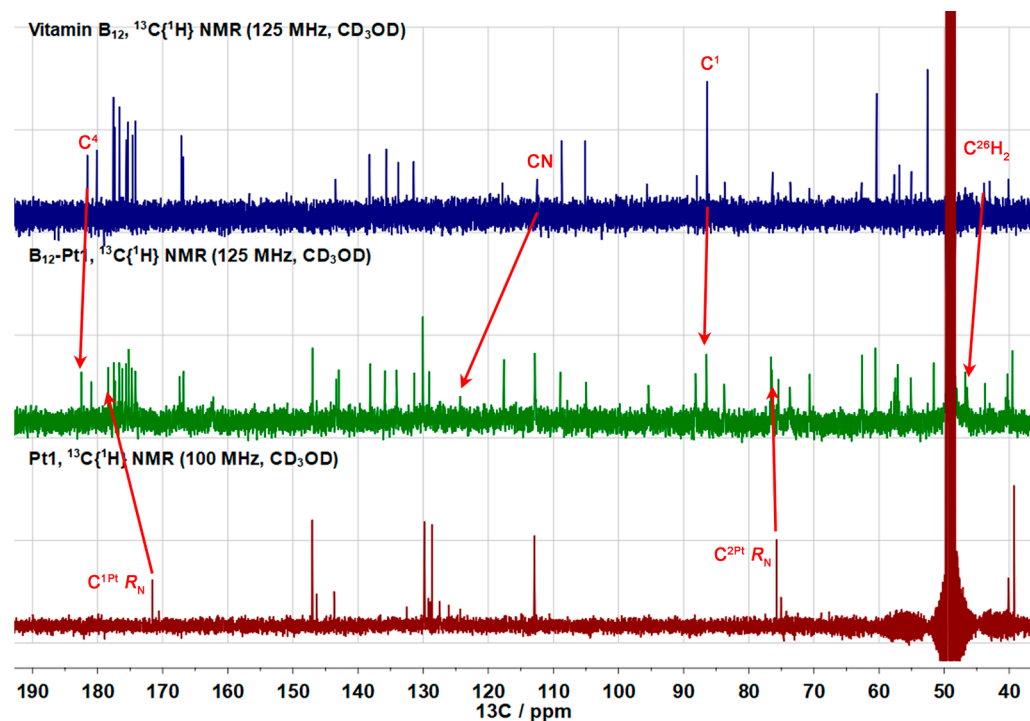


**Figure 6.** Comparison of the  $^{13}\text{C}\{^1\text{H}\}$  NMR spectra in  $\text{CD}_3\text{OD}$  of **Pt1** (bottom), the corresponding vitamin  $\text{B}_{12}$ –platinum(II) conjugate **B<sub>12</sub>-Pt1** (middle), and vitamin  $\text{B}_{12}$  (top) in the range of 40–190 ppm.

Once again, IR spectroscopy proved to be useful to confirm the generation of the expected compounds, with the most informative band being the  $\text{C}\equiv\text{N}$  stretching vibration. The presence of a cyano bridge between two transition metal ions is generally accompanied by a shift of the  $\nu(\text{C}\equiv\text{N})$  to higher wavenumbers compared with the terminal metal–CN counterpart, although exceptions have been reported [54]. This experimental evidence is usually ascribed to the limited mobility of the bridging cyano group due to the mechanical constraint caused by the attachment of a second metal center to the  $N$ -terminus, although the involvement of electrostatic factors cannot be ruled out, and there is evidence that such increase may originate from the depletion of electron density in the weakly antibonding highest occupied molecular orbital (HOMO) of the  $-\text{CN}-$  moiety because of the  $\sigma$ -donating action of the nitrogen end of the cyano ligand towards the second metal center [55]. The involvement of the nitrogen lone pair of the cyano group (mostly residing in the CN antibonding HOMO) in the formation of a CN–Pt(II) bond would induce a withdrawal of charge from the nitrogen to the Pt(II) center. Therefore, the strength of the  $\text{C}\equiv\text{N}$  bond would increase, and that of the Co(III)–C bond would decrease. Thus, compared with the terminal cyano group of vitamin  $\text{B}_{12}$ , the  $\nu(\text{C}\equiv\text{N})$  and the  $\nu(\text{Co(III)}-\text{CN})$  in the cyano-bridged dinuclear complex would be recorded at higher and lower energies, respectively. Accordingly, in the mid-IR spectra of both **B<sub>12</sub>-Pt1** and **B<sub>12</sub>-Pt2**, the  $\nu(\text{C}\equiv\text{N})$  band was recorded at 2197 and 2206  $\text{cm}^{-1}$ , respectively, showing a large shift to higher wavenumbers with respect to the same vibration recorded for the starting cyanocobalamin at 2138  $\text{cm}^{-1}$  [56–58]. The remaining bands substantially resembled those recorded in the same range for the starting reagents vitamin  $\text{B}_{12}$ , **Pt1**, and **Pt2**, with the only exception of two new bands recorded at ca. 1400 and 835  $\text{cm}^{-1}$  being assigned to  $\nu_a(\text{NO}_3^-)$  and  $w(\text{NO}_3^-)$ , respectively [59], which confirmed the presence of the nitrate counter-ion (Figure 7).

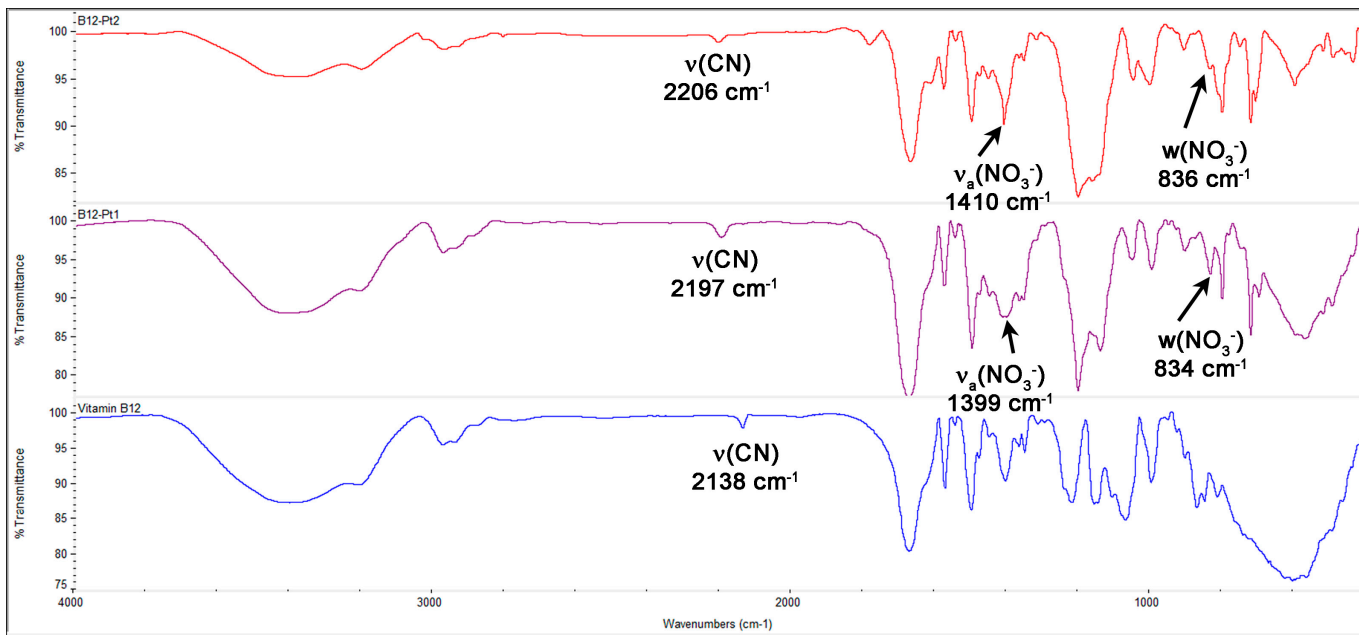


**Figure 7.** Comparison of the mid-IR spectra in CsI of vitamin B<sub>12</sub> (bottom) and the corresponding platinum(II) conjugates B<sub>12</sub>-Pt1 (middle) and B<sub>12</sub>-Pt2 (top).

The bands recorded in the far-IR range (Figure 8) could only be tentatively assigned on the basis of the little data available in the literature, as well as by comparison with the far-IR spectra of the starting platinum(II) complexes Pt1 and Pt2 (see, for example, Figure 4). The most interesting aspect relates to the  $\nu(\text{Co}-\text{CN})$  vibration, which appears at lower wavelengths (*ca.* 392  $\text{cm}^{-1}$ ) in B<sub>12</sub>-Pt1/B<sub>12</sub>-Pt2 compared with the same vibration in free cyanocobalamin (409  $\text{cm}^{-1}$ ), which is in agreement with what was previously discussed in terms of the decrease in strength in the Co(III)–C bond upon the formation of the bridging Co(III)–CN–Pt(II) scaffold [57,58]. Additionally, a new band recorded in the spectra of B<sub>12</sub>-Pt1 and B<sub>12</sub>-Pt2 at *ca.* 435  $\text{cm}^{-1}$  was assigned to the  $\nu(\text{Pt}-\text{NC})$  vibration [57,60].

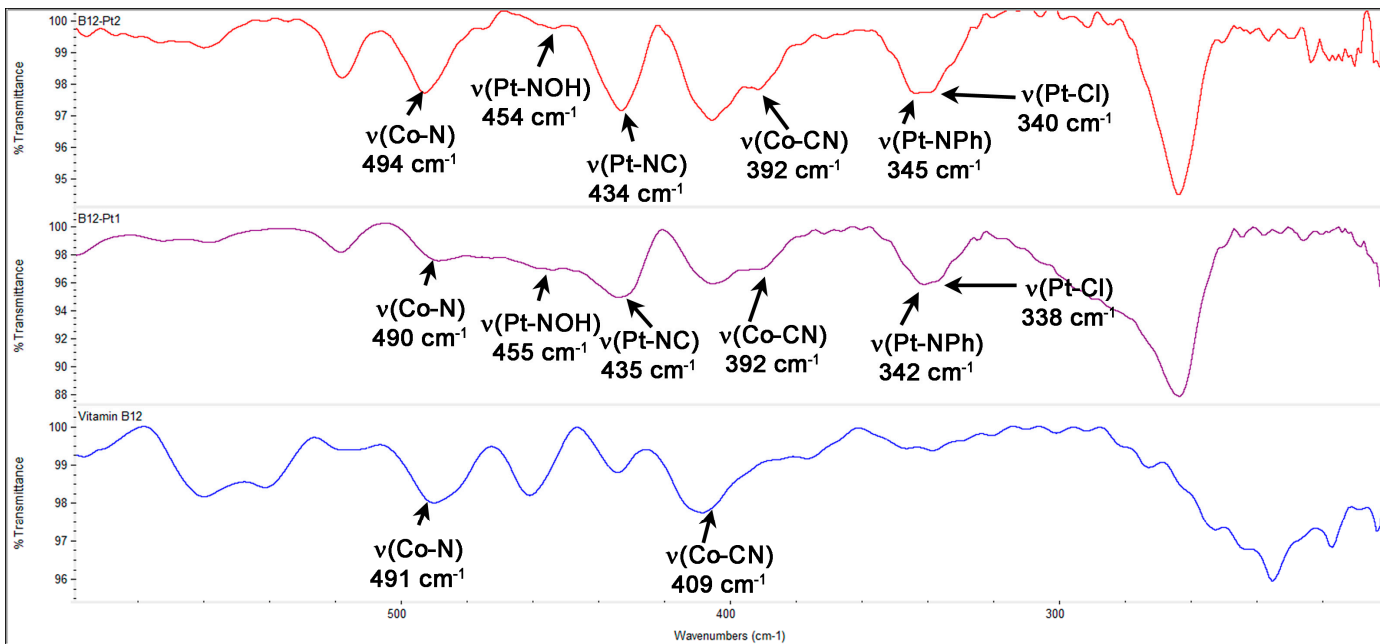
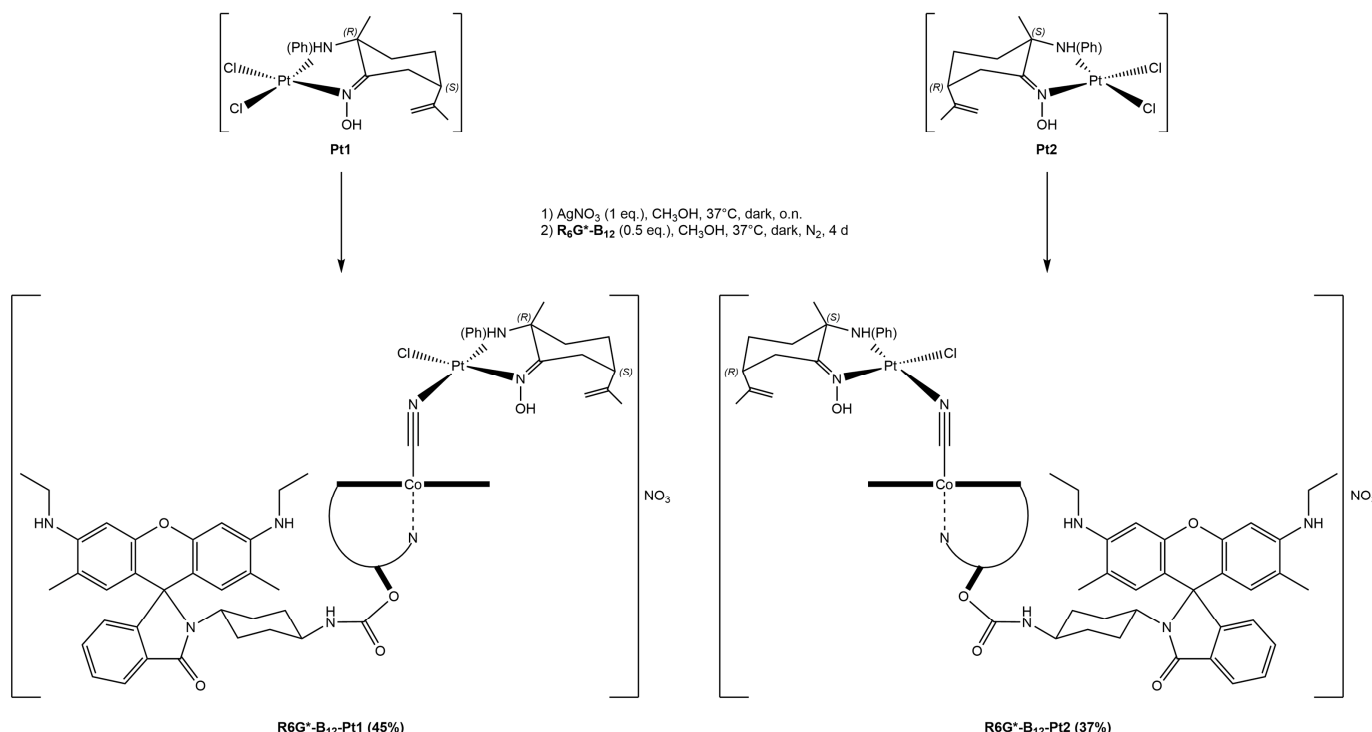


**Figure 8.** Comparison of the far-IR spectra in CsI of vitamin B<sub>12</sub> (bottom) and the corresponding platinum(II) conjugates B<sub>12</sub>-Pt1 (middle) and B<sub>12</sub>-Pt2 (top).

### 2.1.4. Fluorescent Vitamin B<sub>12</sub>–Platinum(II) Derivatives

The target fluorescent vitamin B<sub>12</sub>–platinum(II) derivatives were obtained as previously described in Section 2.1.3. As shown in Scheme 5, the metal precursor (either **Pt1** or **Pt2**) was first treated with 1 eq. of AgNO<sub>3</sub>, the insoluble residue AgCl was filtered off, and the resulting filtrate was reacted with 0.5 eq. of vitamin B<sub>12</sub> at 37 °C in the dark for four days. The solvent was then evaporated under reduced pressure, and the crude product was purified by semi-preparative reversed-phase HPLC, yielding the expected fluorescent vitamin B<sub>12</sub>–platinum(II) conjugates in low to moderate yields (**R6G\*-B<sub>12</sub>-Pt1**: 45%; **R6G\*-B<sub>12</sub>-Pt2**: 37%). The composition of the final compounds was confirmed by HRMS, which returned the peaks of [M-NO<sub>3</sub> + H]<sup>2+</sup> (calcd. 1190.4815 *m/z*) and [M-NO<sub>3</sub> + 2H]<sup>3+</sup> (calcd. 793.9901 *m/z*) at 1189.9517/793.6382 *m/z* and 1190.4873/793.9953 *m/z* for **R6G\*-B<sub>12</sub>-Pt1** and **R6G\*-B<sub>12</sub>-Pt2**, respectively.



**Scheme 5.** Synthesis of the target fluorescent vitamin B<sub>12</sub>–platinum(II) complexes **R6G\*-B<sub>12</sub>-Pt1** and **R6G\*-B<sub>12</sub>-Pt2**.

The IR and NMR spectra of the **R6G\*-B<sub>12</sub>-Pt1** and **R6G\*-B<sub>12</sub>-Pt2** derivatives consistently matched the combined spectra of the starting reagents **R6G\*-B<sub>12</sub>** and **B<sub>12</sub>-Pt1/2**, showing the same spectroscopic features that were previously discussed for the non-fluorescent cyanocobalamin–platinum(II) analogues with very minor deviations (see Section 2.1.3 and Supplementary Materials for details). In particular, in their respective mid-IR spectra, both presented the  $\nu(C\equiv N)$  vibration band at ca. 2200 cm<sup>-1</sup> (**R6G\*-B<sub>12</sub>-Pt1**: 2197 cm<sup>-1</sup>; **R6G\*-B<sub>12</sub>-Pt2**: 2199 cm<sup>-1</sup>) and a <sup>13</sup>C NMR signal at ca. 125 ppm (**R6G\*-B<sub>12</sub>-Pt1**: 125.4 ppm; **R6G\*-B<sub>12</sub>-Pt2**: 124.0 ppm) originated from the CN group, which was consistent with the successful coordination of the cyano moiety of vitamin B<sub>12</sub> to the platinum(II) scaffolds. Moreover, notwithstanding the complexity of the spectra, performing <sup>1</sup>H NMR spectroscopy in CD<sub>3</sub>OD allowed the rough estimate of a 2.5:1 R<sub>N</sub>:S<sub>N</sub> ratio for **R6G\*-B<sub>12</sub>-Pt1** and a 2.1:1 S<sub>N</sub>:R<sub>N</sub> ratio for **R6G\*-B<sub>12</sub>-Pt2** obtained.

## 2.2. Fluorescence Measurements

The absorption and emission spectra of the ligands and the corresponding platinum(II) derivatives are reported in the Supplementary Materials, whereas their optical properties are summarized in Table 1.

**Table 1.** Fluorescence data of vitamin B<sub>12</sub>-platinum(II) derivatives **B<sub>12</sub>-Pt1**, **B<sub>12</sub>-Pt2**, **R6G\*-B<sub>12</sub>-Pt1**, and **R6G\*-B<sub>12</sub>-Pt2** 25 μM in DMSO.

Compound	λ <sub>ex</sub> <sup>em</sup> (nm)	λ <sub>max</sub> <sup>em</sup> (nm)	Stokes Shift (nm)
vitamin B <sub>12</sub>	388	433	45
<b>B<sub>12</sub>-Pt1</b>	367	416	49
<b>B<sub>12</sub>-Pt2</b>	368	413	45
<b>R6G</b>	543	567	24
<b>R6G*</b>	326	563	237
<b>R6G*-B<sub>12</sub></b>	306	420	114
<b>R6G*-B<sub>12</sub>-Pt1</b>	307	412	105
<b>R6G*-B<sub>12</sub>-Pt2</b>	304	414	110

### 2.2.1. Fluorescence Properties of Vitamin B<sub>12</sub>

Vitamin B<sub>12</sub> is a typical example of a poorly fluorescent biomolecule, showing low intensity emission in the long wavelength region. Several methods have been reported to date to identify, quantify, and track cyanocobalamin, including optical spectroscopy, chemiluminescence, surface plasmon resonance, Raman spectroscopy, as well as absorption and fluorescence spectroscopy [61]. Although vitamin B<sub>12</sub> is an inadequate luminescent species, its presence in solution can be detected indirectly through interaction with light-emitting molecules, such as acridine orange, rhodamine 6G, and 4-N,N-di(2-hydroxyethyl)imino-7-nitrobenzo-2-oxa-1,3-diazole (HINBD) [62,63]. In all cases, vitamin B<sub>12</sub> has been shown to quench the fluorescence of the object fluorophores, thus allowing its indirect detection by fluorescence-based analytical techniques.

Both the absorption and emission spectra of vitamin B<sub>12</sub> were obtained in DMSO. Peaks recorded at 279, 304, 338, and 388 (maximum intensity) nm are generally assigned to π→π\* electronic transitions arising from the corrin ring [64]. Upon the excitation of the sample at 388 nm, the scanning of the region from 400 to 700 nm revealed the weak emission spectral profile of cyanocobalamin. Although the same transitions are the most favorable for both absorption and emission processes, the fluorescence spectrum of vitamin B<sub>12</sub> does not adhere to the mirror image rule, which is valid only if referred to S<sub>0</sub>→S<sub>1</sub> (absorption) and S<sub>1</sub>→S<sub>0</sub> (emission) transitions. This is consistent with the fact that, although being the most intense, the absorption band at 388 nm (λ<sub>ex</sub>) does not refer to one S<sub>0</sub>→S<sub>1</sub> electronic transition [65]. Accordingly, in the emission spectrum of vitamin B<sub>12</sub>, only a broad band with a maximum at 433 nm (λ<sub>max</sub><sup>em</sup>) and a very low intensity band at 578 nm are recorded, accounting for a Stokes shift value of 45 nm.

### 2.2.2. Fluorescence Properties of Rhodamine 6G and its Vitamin B<sub>12</sub> Conjugate

Although vitamin B<sub>12</sub> itself has poor photophysical properties (small Stokes shift, low quantum yield, and a tendency to self-quenching) [66], its essential biological role and involvement in diseases such as cancer have been triggering major interest in the development of analytical approaches aimed at probing its trafficking. In particular, fluorescent cobalamin analogues have been designed, in which suitable fluorophores are attached to cyanocobalamin [67]. As previously anticipated, one way to make vitamin B<sub>12</sub> fluorescent is to functionalize it at the 5'-site of its ribose unit with suitable fluorophores. Amongst others, rhodamine 6G (**R6G**) is widely used as dye for fluorescence probes. In aqueous solutions, it shows S<sub>0</sub>→S<sub>1</sub> absorption in the 500–550 nm region (λ<sub>max</sub><sup>ex</sup> ≈ 530 nm) and its fluorescence ranges from 550 to 590 nm (λ<sub>max</sub><sup>em</sup> ≈ 565 nm) [68]. Its remarkably high photostability, high fluorescence quantum yield (0.95), and low cost make it one of the most used fluorescent dyes for a number of applications [69–71].

Rhodamine 6G is the ethyl-esterified derivative of rhodamine 10, and it was developed in such a way to prevent cyclization between the carboxyl function and the xanthene carbon atom C<sup>9</sup>, thus providing remarkable photostability in a wide range of experimental conditions [72], although its sensitivity to pH changes as its fluorescence intensity decreases under acidic conditions [73]. In order to establish a reference point for the subsequent measurements, the absorption and emission spectra of the starting rhodamine 6G were recorded in DMSO. The S<sub>0</sub>→S<sub>1</sub> absorption was observed at  $\lambda_{\text{max}}^{\text{ex}} = 544$  nm, and upon the excitation of the sample at 544 nm, a maximum emission band was recorded at  $\lambda_{\text{max}}^{\text{em}} = 563$  nm, which is in agreement with the data in the literature [74].

As discussed in Section 2.1.1, the rationale of inserting a rigid linker (i.e., a cyclohexane ring) connecting rhodamine 6G and cyanocobalamin relies on the attempt to orient the former away from the corrin ring of cobalamin to minimize through-space intramolecular interactions that would cause fluorescence quenching due to the overlap of the electronic orbital of cobalamin and the excited state of the fluorophore. In our case, this led to the generation of the rhodamine 6G-*trans*-1,4-diaminocyclohexane intermediate (**R6G\***, Scheme 1) whose absorption and emission spectra are reported in the Supplementary Materials. Remarkably, the fluorescence profile of **R6G\*** looks completely different with respect to the starting rhodamine 6G. Three distinct sets of absorptions were recorded at 287, 326 (maximum intensity), and 381 nm. Upon the excitation of the sample at 326 nm, two emission bands were observed at 478 and 565 ( $\lambda_{\text{max}}^{\text{em}}$ ) nm. Such a major difference may be attributed to the cyclization occurring between the amide nitrogen atom (arising from the one end of the *trans*-1,4-diaminocyclohexane linker bound to the 2'-carbonyl function of rhodamine) and the xanthene carbon atom C<sup>9</sup>, leading to the generation of the corresponding lactam (as confirmed by the X-ray structure reported in Figure 3) [75].

Further changes were observed upon conjugating **R6G\*** to vitamin B<sub>12</sub> to generate the fluorescent vitamin B<sub>12</sub> intermediate **R6G\*-B<sub>12</sub>** (Scheme 2), for which absorption and emission maxima were recorded at 306 and 414 nm, respectively. Interestingly, this experimental evidence is not consistent with the data reported in the literature for the (alleged) same conjugate (in ethanol:  $\lambda_{\text{max}}^{\text{ex}} = 530$  nm;  $\lambda_{\text{max}}^{\text{em}} = 5554$  nm) [28].

### 2.2.3. Fluorescence Properties of the Vitamin B<sub>12</sub>-Platinum(II) Derivatives

Both the model and rhodamine 6G-functionalized vitamin B<sub>12</sub>-platinum(II) complexes were studied for their fluorescence profiles, and their optical properties are summarized in Table 1.

The overall absorption/emission profile of vitamin B<sub>12</sub> is substantially maintained in complexes **B<sub>12</sub>-Pt1** and **B<sub>12</sub>-Pt2**, although a substantial shift to shorter wavelengths is observed for both  $\lambda_{\text{max}}^{\text{ex}}$  (from 388 to 367/368 nm) and  $\lambda_{\text{max}}^{\text{em}}$  (from 433 to 416/413 nm) due to the coordination of the platinum(II) scaffolds to the cyano group of vitamin B<sub>12</sub>. In contrast, complexes **R6G\*-B<sub>12</sub>-Pt1** and **R6G\*-B<sub>12</sub>-Pt2** exhibit emission maxima at 412/414 nm ( $\lambda_{\text{max}}^{\text{ex}} = 307/304$  nm), which are fully consistent with the same bands recorded for the fluorescent intermediate **R6G\*-B<sub>12</sub>**, which is indicative of the fact that the coordination of platinum(II) scaffolds does not affect the fluorescence properties of the fluorophore.

### 2.3. Lipophilicity Studies ( $\log D_{7.4}$ )

Lipophilicity is normally expressed as the partition (*P*) or distribution (*D*) coefficient of a substance between two non-miscible phases, mimicking the lipid bilayer of the cell membrane and extra/intracellular environment. In particular, the *n*-octanol/PBS distribution coefficient ( $D_{7.4}$ , defined as the ratio of the molar concentrations of a compound in the *n*-octanol phase and in an aqueous medium phase at pH 7.4) is commonly acknowledged as a representative indication of the distribution under physiological conditions [76]. Log  $D_{7.4}$  is one of the key physicochemical properties to consider in drug discovery because it is related to the bioavailability of a substance [77].

Accordingly, the distribution coefficient of all of the vitamin B<sub>12</sub>-platinum(II) complexes was calculated using the shake-flask method in which an aqueous solution (phosphate-

buffered saline (PBS) solution at pH 7.4) of each tested compound (pre-dissolved in a minimum amount of DMSO which did not interfere with the final estimation of lipophilicity) was mixed with a non-miscible organic solvent (*n*-octanol) and shaken mechanically [78]. Eventually, the two phases were separated by centrifugation, and the concentration of each individual vitamin B<sub>12</sub>–platinum(II) conjugate was derived by measuring the absorbance at 361 nm after partitioning, which allowed the calculation of the respective log  $D_{7.4}$  values.

As summarized in Table 2, the model vitamin B<sub>12</sub>–platinum(II) complexes **B<sub>12</sub>-Pt1** and **B<sub>12</sub>-Pt2** tend to distribute more in the aqueous phase rather than in octanol. In contrast, their fluorescent counterparts, **R6G\*-B<sub>12</sub>-Pt1** and **R6G\*-B<sub>12</sub>-Pt2**, show positive log  $D_{7.4}$  values and, thus, greater lipophilicity. This is consistent with the fact that the conjugation of the rhodamine 6G-*trans*-1,4-diaminocyclohexane scaffold **R6G\*** (which is expected to be less hydrophilic in the lactam form than in its native non-cyclic form) increases the overall lipophilicity of the target cyanocobalamin–metal conjugates. In perspective, such lipophilic nature of **R6G\*-B<sub>12</sub>-Pt1** and **R6G\*-B<sub>12</sub>-Pt2** might indicate that their cell internalization by passive diffusion could not be ruled out.

**Table 2.** Log  $D_{7.4}$  (*n*-octanol/PBS) values calculated for vitamin B<sub>12</sub>–platinum(II) derivatives **B<sub>12</sub>-Pt1**, **B<sub>12</sub>-Pt2**, **R6G\*-B<sub>12</sub>-Pt1**, and **R6G\*-B<sub>12</sub>-Pt2**.

Compound	Log $D_{7.4} \pm$ S.D.
<b>B<sub>12</sub>-Pt1</b>	$-0.81 \pm 0.04$
<b>B<sub>12</sub>-Pt2</b>	$-0.78 \pm 0.05$
<b>R6G*-B<sub>12</sub>-Pt1</b>	$0.52 \pm 0.01$
<b>R6G*-B<sub>12</sub>-Pt2</b>	$0.50 \pm 0.02$

## 2.4. In Vitro Biological Studies

### 2.4.1. Confocal Microscopy

The cell internalization of the tested compounds was evaluated by confocal microscopy. The intracellular accumulation of red fluorescence originating from the vitamin B<sub>12</sub>–platinum(II) conjugates **R6G\*-B<sub>12</sub>-Pt1/2** and the starting fluorophore **R6G** was evident after PC-3 cells incubation for 24 h at 37 °C (Figure 9). After 72 h, the bright emission of metal derivatives and rhodamine 6G was detected throughout the cells, but no significant co-localization with the blue luminescence of Hoechst (a nucleus dye) was observed, which either means the compounds did not enter the nucleus or their emission was quenched there.

Since cyanocobalamin is taken up by cells following a temperature-dependent endocytosis process of the TCII-B<sub>12</sub> complex (holo-TCII) [79], we qualitatively evaluated whether the vitamin B<sub>12</sub>–platinum(II) conjugates would also be internalized through an energy-dependent mechanism. Notably, the confocal microscopy images of both metal conjugates possess a granular pattern reminiscent of vesicles that are widely distributed in cells. Since energy-dependent pathways, such as endocytosis, are inhibited at low temperatures [80], cultured PC-3 cells were incubated with **R6G\*-B<sub>12</sub>-Pt1** at 37 °C and 4 °C for 3 h. The confocal microscopy images showed red emissions in the cytoplasmic region due to metal conjugates only for the experiment carried out at 37 °C (Figure 10), supporting the hypothesis of the involvement of an energy-dependent pathway taking place for the uptake of fluorescent vitamin B<sub>12</sub>–platinum(II) complexes.

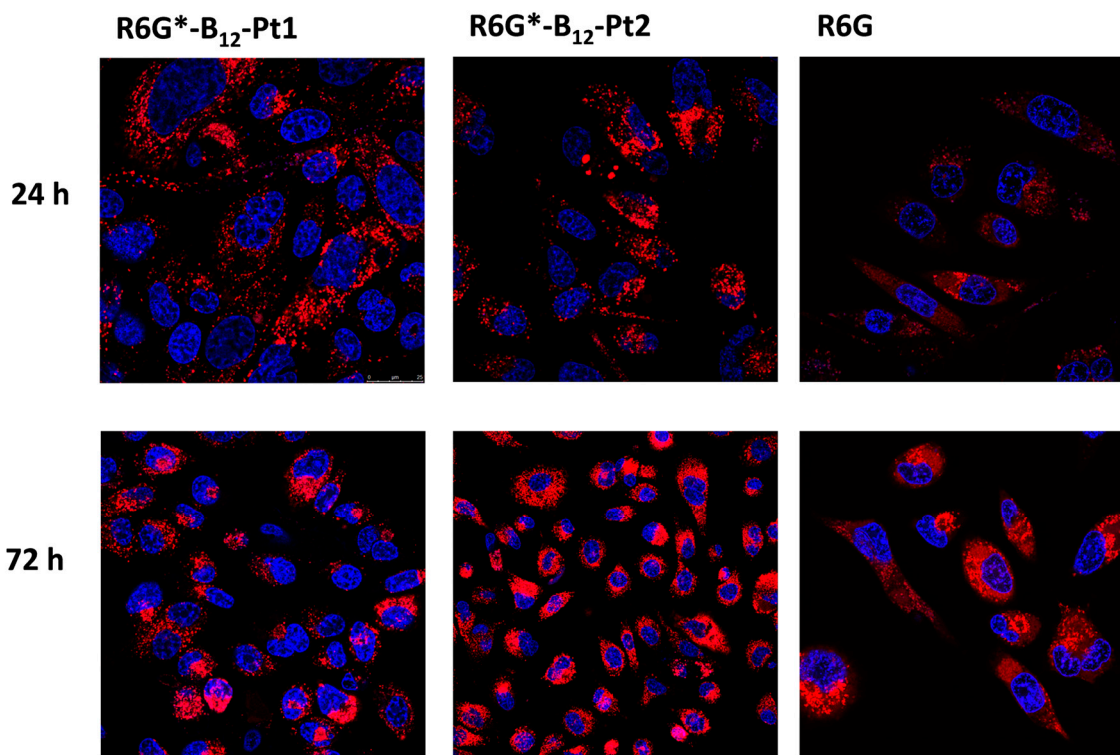


**Figure 9.** Confocal microscopy images of PC-3 cells incubated with either R6G\*-B<sub>12</sub>-Pt1, R6G\*-B<sub>12</sub>-Pt2, or R6G (10  $\mu$ M) for 24 and 72 h at 37  $^{\circ}$ C after excitation at 563 nm.

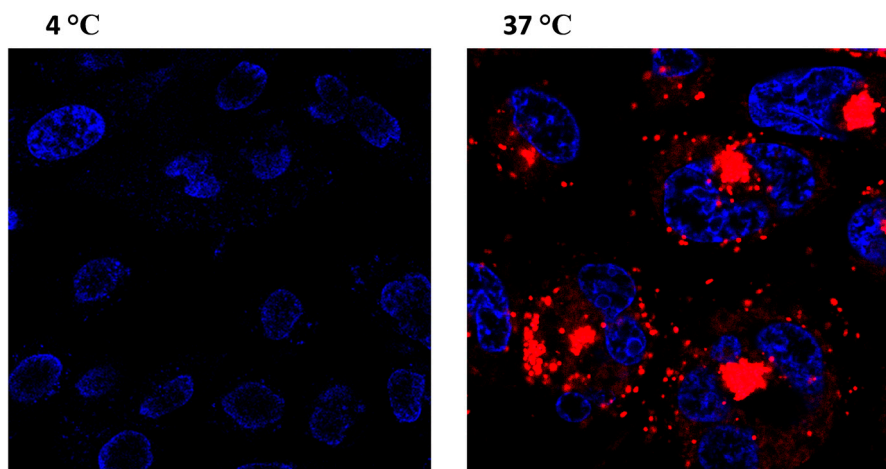


**Figure 10.** Confocal microscopy images of PC-3 cells incubated with R6G\*-B<sub>12</sub>-Pt1 (200  $\mu$ M) for 3 h at 4  $^{\circ}$ C and 37  $^{\circ}$ C after excitation at 563 nm.

#### 2.4.2. Antiproliferative Activity

The capability of the starting platinum(II) complexes (**Pt1** and **Pt2**) and their vitamin B<sub>12</sub> conjugates, both non-fluorescent (**B<sub>12</sub>-Pt1** and **B<sub>12</sub>-Pt2**) and fluorescent (**R6G\*-B<sub>12</sub>-Pt1** and **R6G\*-B<sub>12</sub>-Pt2**), to inhibit cell growth was assayed on three human tumor cell lines, namely prostate cancer (PC-3), cervical carcinoma (HeLa), and breast adenocarcinoma (MCF-7) cells, they are obtained from the American Type Culture Collection (Manassas, VA). As the first clinically approved anticancer metallodrug, cisplatin was also evaluated as a reference under the same experimental conditions for comparison purposes, as well as the starting reagents vitamin B<sub>12</sub> and rhodamine 6G. Antiproliferative data, expressed as IC<sub>50</sub> values calculated as the mean of at least three independent experiments, are reported in Table 3.

**Table 3.** Cell growth inhibition data after 72 h of incubation.

Compound	$IC_{50} \pm S.D. (\mu M)$		
	PC-3	HeLa	MCF-7
<b>vitamin B<sub>12</sub></b>	no convergence	no convergence	no convergence
<b>R6G</b>	1.11 ± 1.09	1.95 ± 1.09	1.62 ± 1.22
<b>Pt1</b>	85.9 ± 19.3	>100	>100
<b>Pt2</b>	86.8 ± 4.5	>100	>100
<b>B<sub>12</sub>-Pt1</b>	>100	>100	>100
<b>B<sub>12</sub>-Pt2</b>	>100	>100	>100
<b>R6G*-B<sub>12</sub>-Pt1</b>	47.9 ± 1.0	77.2 ± 1.0	70.3 ± 1.0
<b>R6G*-B<sub>12</sub>-Pt2</b>	42.7 ± 1.0	73.1 ± 1.0	58.1 ± 1.0
<b>B<sub>12</sub>-Pt1 + R6G</b>	2.58 ± 1.15	4.85 ± 1.10	0.80 ± 1.00
<b>cisplatin</b>	16.5 ± 1.1	14.5 ± 2.5	9.80 ± 0.96

The starting platinum(II) complexes **Pt1** and **Pt2** exhibited no (HeLa and MCF-7) or negligible (PC-3) cytotoxic activity, and conjugation to vitamin B<sub>12</sub> did not enhance their antiproliferative profiles.

In agreement with the reports in the literature, rhodamine 6G (**R6G**) proved to be highly cytotoxic against the tested cell lines ( $IC_{50} \approx 1\text{--}2 \mu M$ ) [81,82], and a similar profile was maintained upon the combined treatment of the cells with equimolar amounts of **B<sub>12</sub>-Pt1** and **R6G** ( $IC_{50} \approx 1\text{--}5 \mu M$ ). However, the rhodamine-functionalized analogues **R6G\*-B<sub>12</sub>-Pt1** and **R6G\*-B<sub>12</sub>-Pt2** only showed some (albeit limited and much lower than cisplatin) antiproliferative activity, with  $IC_{50}$  values in the 40–70  $\mu M$  range, and no significant variations were generally observed for the different epimers of the metal scaffold. It can be speculated that the comparatively more lipophilic nature of the fluorescent cyanocobalamin–platinum(II) conjugates (Table 2) would promote cellular uptake via passive diffusion [83]. On the other hand, since the cytotoxicity data are substantially different from those of the non-fluorescent counterparts **B<sub>12</sub>-Pt1** and **B<sub>12</sub>-Pt2**, the cleavage of the vitamin B<sub>12</sub>–rhodamine bond and the subsequent release of the free rhodamine scaffold can be confidently ruled out.

#### 2.4.3. Cell Cycle Assay

The dysregulation of the cell cycle is a hallmark of tumorigenesis [84]. Therefore, the effect on the cell cycle exerted by **R6G\*-B<sub>12</sub>-Pt1** and **R6G\*-B<sub>12</sub>-Pt2** was assessed. PC-3 cells were incubated for 72 h at  $IC_{50}/2$  concentrations of the chosen compounds, and the DNA content was analyzed by flow cytometry after staining with propidium iodide. Rhodamine 6G and cisplatin were also tested under the same experimental conditions for comparison purposes.

The results reported in Figure 11 show no significant changes in the cell cycle populations after exposure to the vitamin B<sub>12</sub>–platinum(II) conjugates, which is consistent with their moderate cytotoxicity (Table 3). In contrast, cisplatin dramatically affected cell distribution in the S phase, in which DNA synthesis takes place, which is in agreement with the data in the literature [85]. Interestingly, rhodamine 6G (**R6G**), a well-known inhibitor of mitochondrial oxidative phosphorylation [86], does not alter the cell cycle population, pointing to a cell death mechanism that is essentially distinct from that of cisplatin.

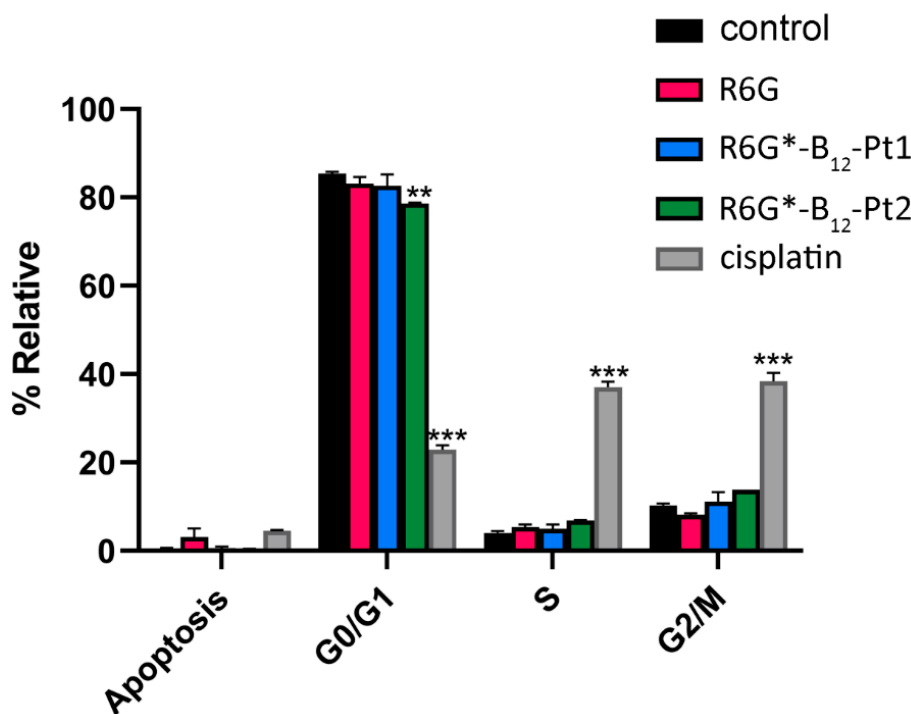


**Figure 11.** Cell cycle distribution of PC-3 cells after incubation for 72 h with either **R6G** (0.5  $\mu$ M), cisplatin (14.5  $\mu$ M), **R6G\*-B<sub>12</sub>-Pt1** (38.6  $\mu$ M), or **R6G\*-B<sub>12</sub>-Pt2** (36.5  $\mu$ M). Results are reported as percentage of cells in each phase of cycle compared to untreated control cells. Data are shown as means  $\pm$  S.D. of four independent experiments \*\*  $p < 0.01$ ; \*\*\*  $p < 0.001$  vs. control.

#### 2.4.4. DNA Interaction

Since DNA is an established cellular target of platinum(II) complexes [87], preliminary evaluations of the interaction between the full set of vitamin B<sub>12</sub>–platinum(II) conjugates and DNA were performed in vitro by means of equilibrium dialysis and FRET-based DNA melting assays.

Equilibrium dialysis assays with CT DNA and **B<sub>12</sub>-Pt1**, **B<sub>12</sub>-Pt2**, **R6G\*-B<sub>12</sub>-Pt1**, and **R6G\*-B<sub>12</sub>-Pt2** derivatives were carried out to assess their binding affinity towards double-stranded DNA. Apparent association constants ( $K_{app}$ ) were determined after 24 h of incubation at room temperature at a near physiological pH following the protocol described by Chaires [88] with some modifications (see Supplementary Materials for details). The association constants obtained for all vitamin B<sub>12</sub> conjugates are in the order of  $10^4 \text{ M}^{-1}$ :  $2.6 \pm 0.2$  (**B<sub>12</sub>-Pt1**),  $2.0 \pm 0.3$  (**B<sub>12</sub>-Pt2**),  $4.1 \pm 0.3$  (**R6G\*-B<sub>12</sub>-Pt1**), and  $2.6 \pm 0.1$  (**R6G\*-B<sub>12</sub>-Pt2**). This indicates that all platinum conjugates bind dsDNA with moderate binding affinity, which is in agreement with the results previously reported for some Pd(II) structural analogues [38]. In addition, conjugation with **R6G\*** does not interfere with DNA recognition. As a matter of fact, the DNA binding affinities of the fluorescent conjugates turned out to be slightly higher than those of the non-fluorescent counterparts, especially in the case of **R6G\*-B<sub>12</sub>-Pt1**.

FRET-based DNA melting assays were performed to identify the occurrence of stabilizing or destabilizing effects on the double-helix DNA secondary structure. The binding of **B<sub>12</sub>-Pt1**, **B<sub>12</sub>-Pt2**, **R6G\*-B<sub>12</sub>-Pt1**, and **R6G\*-B<sub>12</sub>-Pt2** to duplex-forming, dual-labeled (5'-FAM and 3'-TAMRA) short oligonucleotide F10T was evaluated using a wide range of ligand/DNA molar ratios (see Supplementary Materials for details). Under the experimental conditions used, the compounds showed negligible thermal stabilization effects over the annealed structures, which is consistent with a binding mode that might involve a combination of groove and/or electrostatic interactions (see Supplementary Materials, page S69, panel A). Interestingly, when the denatured DNA was allowed to fold in the presence of vitamin B<sub>12</sub> conjugates, subtle thermal destabilizing effects were recorded at higher ligand/DNA molar ratios, with  $\Delta T_m = -1^\circ\text{C}$  for compounds **B<sub>12</sub>-Pt1** and **B<sub>12</sub>-Pt2**

and  $\Delta T_m = -3$  °C for compounds **R6G\*-B<sub>12</sub>-Pt1** and **R6G\*-B<sub>12</sub>-Pt2** (see Supplementary Materials, page S69, panel B). This effect was more pronounced when parallel DNA folding experiments were carried out in a buffer system depleted of chloride ions:  $\Delta T_m = -4$  °C was observed for **B<sub>12</sub>-Pt1**, **R6G\*-B<sub>12</sub>-Pt1**, and **R6G\*-B<sub>12</sub>-Pt2**, whereas the non-fluorescent conjugate **B<sub>12</sub>-Pt2** induced a DNA  $\Delta T_m = -6$  °C (see Supplementary Materials, page S69, panel C), presumably because the coordination of the platinum(II) center to the purine-N(7) of adenine or guanine bases is hastened and the thermal stability of F10T is reduced under such conditions.

### 3. Materials and Methods

Materials, general methods (including instrumentation used), synthetic procedures, complete spectroscopic characterizations (including MS, IR, NMR, and absorption/emission spectra), and crystallographic data are detailed in the Supplementary Materials.

### 4. Conclusions

The goal of the research work reported here was to design fluorescent vitamin B<sub>12</sub>—metal conjugates as theranostic anticancer agents with a focus on their potential targeting capability due to the increased demand for vitamin B<sub>12</sub> by fast-proliferating cancer cells in order to attain tumor selectivity. Four novel cyanocobalamin–platinum(II) derivatives were successfully generated in low-to-medium yields and high purity. All synthesized compounds (including precursors, intermediates, and target metal derivatives) were characterized by means of several analytical techniques, and the results were fully consistent with the expected formulation. The functionalization of vitamin B<sub>12</sub> with a rhodamine-based scaffold yielded fluorescent derivatives (**R6G\*-B<sub>12</sub>-Pt1/2**) showing markedly different emission profiles compared with the starting fluorescent probe rhodamine 6G, as well as with the non-fluorescent model vitamin B<sub>12</sub>–platinum(II) counterparts (**B<sub>12</sub>-Pt1/2**).

The in vitro cytotoxicity was evaluated towards three human tumor cell lines (namely PC-3, HeLa and MCF-7). Although exhibiting low antiproliferative activity ( $IC_{50} = 40$ –70 µM), both **R6G\*-B<sub>12</sub>-Pt1** and **R6G\*-B<sub>12</sub>-Pt2** showed an enhanced capability to inhibit cells viability compared with the inactive ( $IC_{50} > 100$  µM) precursors **Pt1/2** and **B<sub>12</sub>-Pt1/2**, which is possibly due to their higher lipophilicity (promoted by the functionalization of cyanocobalamin with the rhodamine scaffold), which would favor cellular uptake through passive diffusion mechanisms.

In order to gain insights into their mechanism of action, **R6G\*-B<sub>12</sub>-Pt1/2** were subjected to additional biological evaluations. No significant changes in cell cycle populations were recorded after exposure to such vitamin B<sub>12</sub>–platinum(II) conjugates, which is consistent with their moderate cytotoxicity. However, confocal microscopy experiments clearly confirmed that both complexes are indeed internalized into the cells and tend to accumulate in the cytoplasmic region. Remarkably, such accumulation could be observed only at 37 °C but not at a low (4 °C) temperature, indicating that an energy-dependent pathway is involved in the cell uptake of the target fluorescent vitamin B<sub>12</sub>–platinum(II) complexes.

The interaction of **R6G\*-B<sub>12</sub>-Pt1/2** with DNA was preliminarily assessed by equilibrium dialysis and FRET-based DNA melting assays. The vitamin B<sub>12</sub>–platinum(II) conjugates were found to bind CT DNA with apparent association constants of  $4.1 \pm 0.3 \times 10^4$  (**R6G\*-B<sub>12</sub>-Pt1**) and  $2.6 \pm 0.1 \times 10^4$  M<sup>-1</sup> (**R6G\*-B<sub>12</sub>-Pt2**), showing a slightly higher binding affinity than the analogues lacking the fluorescent probe rhodamine 6G. In addition, none of the conjugates were proven to thermally stabilize dsDNA, which is consistent with a binding mode that may involve groove recognition and/or electrostatic interactions. However, mild destabilizing effects were observed during the DNA annealing process at high ligand/DNA ratios, especially under chloride ions depletion, which is in agreement with the structural characteristics of the conjugates and the presence of reactive Pt–Cl bonds.

Although further in-depth studies are required to confirm the hypothesized transport mechanism and to assess additional possible biological targets, the research reported here represents a starting point for the development of this class of fluorescent vitamin B<sub>12</sub>–metal

conjugates. Future experiments would include the determination of their fluorescence quantum yield (using rhodamine 6G as a reference) and antiproliferative tests in the presence of specific transport proteins (e.g., Transcobalamin II) in order verify whether this would facilitate their cell internalization and, thus, improve cytotoxicity.

**Supplementary Materials:** The following supporting information can be downloaded at <https://www.mdpi.com/article/10.3390/inorganics12030091/s1>. Materials and methods (including abbreviations and instrumentation [89–93] used; pages S2–S8); synthesis and spectroscopic characterization (including MS, IR, and NMR [94–102] spectra) of the starting reagents (**B<sub>12</sub>**, **R6G**, **L1**, and **L2**; pages S9–S23), the vitamin **B<sub>12</sub>**-rhodamine 6G adduct (**R6G\*** and **R6G\*-B<sub>12</sub>**; pages S24–S33), the platinum(II) precursors (**Pt1** and **Pt2**; pages S34–S41), the vitamin **B<sub>12</sub>**-platinum(II) conjugates (**B<sub>12</sub>-Pt1**, **B<sub>12</sub>-Pt2**, **R6G\*-B<sub>12</sub>-Pt1**, and **R6G\*-B<sub>12</sub>-Pt2**; pages S42–S63); the UV-Vis spectra (**Pt1** and **Pt2**; page S64); the absorption/emission spectra (**B<sub>12</sub>**, **R6G**, **R6G\***, **R6G\*-B<sub>12</sub>**, **B<sub>12</sub>-Pt1**, **B<sub>12</sub>-Pt2**, **R6G\*-B<sub>12</sub>-Pt1**, and **R6G\*-B<sub>12</sub>-Pt2**; pages S64–S66); the single crystal X-ray diffraction data (**R6G\*** and **R<sub>N</sub>-Pt1**; pages S67–S68); the FRET-DNA melting curves (**B<sub>12</sub>-Pt1**, **B<sub>12</sub>-Pt2**, **R6G\*-B<sub>12</sub>-Pt1**, and **R6G\*-B<sub>12</sub>-Pt2**; page S69); the CIF; and the check-CIF PDF files (CCDC 2321413 (**R6G\***) and 2321414 (**R<sub>N</sub>-Pt1**)).

**Author Contributions:** Conceptualization: L.R. and E.R.; investigation: R.M. (synthesis, characterization, fluorescence, and lipophilicity studies of **R6G\***, **R6G\*-B<sub>12</sub>**, **B<sub>12</sub>-Pt1**, **B<sub>12</sub>-Pt2**, **R6G\*-B<sub>12</sub>-Pt1**, and **R6G\*-B<sub>12</sub>-Pt2**), I.d.l.C.-A. (synthesis and characterization of **Pt1** and **Pt2**), E.d.l.T.-R. (biological experiments), C.O. (X-ray crystallography of **R6G\***), and A.P.-R. (X-ray crystallography of **R<sub>N</sub>-Pt1**); validation: L.R. (chemical and analytical data of vitamin **B<sub>12</sub>**-platinum(II) conjugates), E.R. (chemical and analytical data of platinum(II) complexes), A.P.-R. (X-ray data), E.d.l.T.-R. (biological data), and L.G. (DNA interaction data); writing/original draft preparation: L.R., R.M., E.d.l.T.-R. and E.R.; writing/review and editing: L.R., E.R., L.G. and A.P.-R.; supervision: L.R., L.G., and E.R.; funding acquisition: R.M., E.R. and L.G. All authors have read and agreed to the published version of the manuscript.

**Funding:** The financial support from the Ministry of Education of Saudi Arabia and Saudi Cultural Bureau (Postgraduate Scholarship to R.M.), the Spanish Ministry of Science and Innovation (Project PID2019-108251RB-I00/AEI/10.13039/501100011033 to L.G. and E.R., and Fellowship FPU19/03617 to E.d.l.T.-R.), and the University of Alcalá (Projects UAH-AE-2017-2, GP2023-02, PIUAH22/CC-028, CCG2020/CC-026, and CCG20/CC-007) is gratefully acknowledged.

**Data Availability Statement:** The data presented in this study are available upon request from the corresponding author. The data are not publicly available due to a 24-month embargo period in relation to the pending submission of R.M.’s PhD thesis. The data will be published online at the end of the embargo period in the University of Galway Research Repository ARAN (<https://aran.library.nuigalway.ie/>) in accordance with the FAIR Principles underlined in the University of Galway policy on Open Access to Research Outputs (<https://library.universityofgalway.ie/about/policies/openaccesstoresearchoutputspolicy/#>).

**Conflicts of Interest:** The authors declare no conflicts of interest, financial or otherwise. The funders had no role in the design of the study; in the collection, analyses, or interpretation of data; in the writing of the manuscript; or in the decision to publish the results.

## References

1. Anand, U.; Dey, A.; Chandel, A.K.S.; Sanyal, R.; Mishra, A.; Pandey, D.K.; De Falco, V.; Upadhyay, A.; Kandimalla, R.; Chaudhary, A.; et al. Cancer chemotherapy and beyond: Current status, drug candidates, associated risks and progress in targeted therapeutics. *Genes Dis.* **2022**, *10*, 1367–1401. [[CrossRef](#)]
2. Zhang, C.; Xu, C.; Gao, X.; Yao, Q. Platinum-based drugs for cancer therapy and anti-tumor strategies. *Theranostics* **2022**, *12*, 2115–2132. [[CrossRef](#)]
3. Bedard, P.L.; Hyman, D.M.; Davids, M.S.; Siu, L.L. Small molecules, big impact: 20 years of targeted therapy in oncology. *Lancet* **2020**, *395*, 1078–1088. [[CrossRef](#)]
4. Iqbal, N.; Iqbal, N. Imatinib: A breakthrough of targeted therapy in cancer. *Chemother. Res. Pract.* **2014**, *2014*, 357027. [[CrossRef](#)]
5. Hanahan, D. Hallmarks of cancer: New dimensions. *Cancer Discov.* **2022**, *12*, 31–46. [[CrossRef](#)]
6. Zhong, L.; Li, Y.; Xiong, L.; Wang, W.; Wu, M.; Yuan, T.; Yang, W.; Tian, C.; Miao, Z.; Wang, T.; et al. Small molecules in targeted cancer therapy: Advances, challenges, and future perspectives. *Signal Transduct. Target. Ther.* **2021**, *6*, 201. [[CrossRef](#)]
7. Pettenuzzo, A.; Pigot, R.; Ronconi, L. Vitamin **B<sub>12</sub>**-metal conjugates for targeted chemotherapy and diagnosis: Current status and future prospects. *Eur. J. Inorg. Chem.* **2017**, *12*, 1625–1638. [[CrossRef](#)]

8. Russell-Jones, G.J.; Arthur, L.; Walker, H. Vitamin B<sub>12</sub>-mediated transport of nanoparticles across Caco-2 cells. *Int. J. Pharm.* **1999**, *179*, 247–255. [[CrossRef](#)]
9. Obeid, R.; Heil, S.G.; Verhoeven, M.M.A.; van den Heuvel, E.G.H.M.; de Groot, L.C.P.G.M.; Eussen, S.J.P.M. Vitamin B<sub>12</sub> intake from animal foods, biomarkers, and health aspects. *Front. Nutr.* **2019**, *6*, 93. [[CrossRef](#)]
10. Nielsen, M.J.; Rasmussen, M.R.; Andersen, C.B.; Nexø, E.; Moestrup, S.K. Vitamin B<sub>12</sub> transport from food to the body's cells—A sophisticated, multistep pathway. *Nat. Rev. Gastroenterol. Hepatol.* **2012**, *9*, 345–354. [[CrossRef](#)]
11. Gendron, L.N.; Zites, D.C.; LaRochelle, E.P.M.; Gunn, J.R.; Pogue, B.W.; Shell, T.A.; Shell, J.R. Tumor targeting vitamin B<sub>12</sub> derivatives for X-ray induced treatment of pancreatic adenocarcinoma. *Photodiagn. Photodyn. Ther.* **2020**, *30*, 101637. [[CrossRef](#)] [[PubMed](#)]
12. Mundwiler, S.; Spingler, B.; Kurz, P.; Kunze, S.; Alberto, R. Cyanide-bridged vitamin B<sub>12</sub>-cisplatin conjugates. *Chem. Eur. J.* **2005**, *11*, 4089–4095. [[CrossRef](#)]
13. Ruiz-Sánchez, P.; Mundwiler, S.; Spingler, B.; Buan, N.R.; Escalante-Semerena, J.C.; Alberto, R. Syntheses and characterization of vitamin B<sub>12</sub>-Pt(II) conjugates and their adenosylation in an enzymatic assay. *J. Biol. Inorg. Chem.* **2008**, *13*, 335–347. [[CrossRef](#)] [[PubMed](#)]
14. Ruiz-Sánchez, P.; König, C.; Ferrari, S.; Alberto, R. Vitamin B<sub>12</sub> as a carrier for targeted platinum delivery: In vitro cytotoxicity and mechanistic studies. *J. Biol. Inorg. Chem.* **2011**, *16*, 33–44. [[CrossRef](#)] [[PubMed](#)]
15. Tran, M.T.Q.; Furger, E.; Alberto, R. Two-step activation prodrugs: Transplatin mediated binding of chemotherapeutic agents to vitamin B<sub>12</sub>. *Org. Biomol. Chem.* **2013**, *11*, 3247–3254. [[CrossRef](#)] [[PubMed](#)]
16. Tran, M.T.Q.; Stürup, S.; Lambert, I.H.; Gammelgaard, B.; Furger, E.; Alberto, R. Cellular uptake of metallated cobalamins. *Metallomics* **2016**, *8*, 298–304. [[CrossRef](#)] [[PubMed](#)]
17. Kunze, S.; Zobi, F.; Kurz, P.; Spingler, B.; Alberto, R. Vitamin B<sub>12</sub> as a ligand for technetium and rhenium complexes. *Angew. Chem. Int. Ed.* **2004**, *43*, 5025–5029. [[CrossRef](#)] [[PubMed](#)]
18. Rossier, J.; Hauser, D.; Kottelat, E.; Rothen-Rutishauser, B.; Zobi, F. Organometallic cobalamin anticancer derivatives for targeted prodrug delivery via transcobalamin-mediated uptake. *Dalton Trans.* **2017**, *46*, 2159–2164. [[CrossRef](#)]
19. Atoum, M.F.; Alzoughool, F.E.; Al-Mazaydeh, Z.A.; Rammaha, M.S.; Tahtamouni, L.H. Vitamin B<sub>12</sub> enhances the antitumor activity of 1,25-dihydroxyvitamin D<sub>3</sub> via activation of caspases and targeting actin cytoskeleton. *Tumor Biol.* **2022**, *44*, 17–35. [[CrossRef](#)]
20. McGreevy, J.M.; Cannon, M.J.; Grissom, C.B. Minimally invasive lymphatic mapping using fluorescently labeled vitamin B<sub>12</sub>. *J. Surg. Res.* **2003**, *111*, 38–44. [[CrossRef](#)]
21. Fedosov, S.N.; Grissom, C.B.; Fedosova, N.U.; Moestrup, S.K.; Nexø, E.; Petersen, T.E. Application of a fluorescent cobalamin analogue for analysis of the binding kinetics. A study employing recombinant human transcobalamin and intrinsic factor. *FEBS J.* **2006**, *273*, 4742–4753. [[CrossRef](#)] [[PubMed](#)]
22. Vortherms, A.R.; Kahkoska, A.R.; Rabideau, A.E.; Zubietta, J.; Andersen, L.L.; Madsen, M.; Doyle, R.P. A water soluble vitamin B<sub>12</sub>-Re(I) fluorescent conjugate for cell uptake screens: Use in the confirmation of cubilin in the lung cancer line A549. *Chem. Commun.* **2011**, *47*, 9792–9794. [[CrossRef](#)]
23. Wuerges, J.; Garau, G.; Geremia, S.; Fedosov, S.N.; Petersen, T.E.; Randaccio, L. Structural basis for mammalian vitamin B<sub>12</sub> transport by transcobalamin. *Proc. Natl. Acad. Sci. USA* **2006**, *103*, 4386–4391. [[CrossRef](#)] [[PubMed](#)]
24. Petrus, A.K.; Vortherms, A.R.; Fairchild, T.J.; Doyle, R.P. Vitamin B<sub>12</sub> as a carrier for the oral delivery of insulin. *ChemMedChem* **2007**, *2*, 1717–1721. [[CrossRef](#)] [[PubMed](#)]
25. Wang, X.; Wei, L.; Kotra, L.P. Cyanocobalamin (vitamin B<sub>12</sub>) conjugates with enhanced solubility. *Bioorg. Med. Chem.* **2007**, *15*, 1780–1787. [[CrossRef](#)] [[PubMed](#)]
26. Chang, P.V.; Chen, X.; Smyrniotis, C.; Xenakis, A.; Hu, T.; Bertozzi, C.R.; Wu, P. Metabolic labeling of sialic acids in living animals with alkynyl sugars. *Angew. Chem. Int. Ed.* **2009**, *48*, 4030–4033. [[CrossRef](#)]
27. Clardy, S.M.; Allis, D.G.; Fairchild, T.J.; Doyle, R.P. Vitamin B<sub>12</sub> in drug delivery: Breaking through the barriers to a B<sub>12</sub> bioconjugate pharmaceutical. *Expert Opin. Drug Deliv.* **2011**, *8*, 127–140. [[CrossRef](#)]
28. Lee, M.; Grissom, C.B. Design, synthesis, and characterization of fluorescent cobalamin analogues with high quantum efficiencies. *Org. Lett.* **2009**, *11*, 2499–2502. [[CrossRef](#)]
29. Mchedlov-Petrosyan, N.O.; Fedorov, L.A.; Sokolovskii, S.A.; Surov, Y.N.; Salinas Maiorga, R. Structural conversions of rhodamines in solution. *Russ. Chem. Bull.* **1992**, *41*, 403–409. [[CrossRef](#)]
30. Bhanja, A.K.; Mishra, S.; Naskar, K.; Maity, S.; Das Saha, K.; Sinha, C. Specific recognition of Cr<sup>3+</sup> under physiological conditions by allyl substituted appendage rhodamine and its cell-imaging studies. *Dalton Trans.* **2017**, *46*, 16516–16524. [[CrossRef](#)]
31. Lu, D.; Yang, T.; Tang, N.; Li, C.; Song, Y.; Wang, L.; Wong, W.Y.; Yin, S.F.; Xing, Y.; Kambe, N.; et al. A pH-dependent rhodamine fluorophore with antiproliferative activity of bladder cancer in vitro/vivo and apoptosis mechanism. *Eur. J. Med. Chem.* **2022**, *236*, 114293. [[CrossRef](#)] [[PubMed](#)]
32. Majoube, M.; Henry, M. Fourier transform Raman and infrared and surface-enhanced Raman spectra for rhodamine 6G. *Spectrochim. Acta A* **1991**, *47*, 1459–1466. [[CrossRef](#)]
33. Alkadi, H.; Jbeily, R. Role of chirality in drugs: An overview. *Infect. Disord. Drug Targets* **2018**, *18*, 88–95. [[CrossRef](#)] [[PubMed](#)]
34. Arnesano, F.; Pannunzio, A.; Coluccia, M.; Natile, G. Effect of chirality in platinum drugs. *Coord. Chem. Rev.* **2015**, *284*, 286–297. [[CrossRef](#)]

35. Pacuła-Miszewska, A.J.; Obieziurska-Fabiszak, M.; Ścianowski, J. Monoterpenes as chiral building blocks. In *Chiral Building Blocks in Asymmetric Synthesis: Synthesis and Applications*; Wojaczyńska, E., Wojaczyński, J., Eds.; Wiley-VCH: Weinheim, Germany, 2022; pp. 235–266.
36. de la Cueva-Alique, I.; Sierra, S.; Muñoz-Moreno, L.; Pérez-Redondo, A.; Bajo, A.M.; Marzo, I.; Gude, L.; Cuenca, T.; Royo, E. Biological evaluation of water soluble arene Ru(II) enantiomers with amino-oxime ligands. *J. Inorg. Biochem.* **2018**, *183*, 32–42. [[CrossRef](#)] [[PubMed](#)]
37. Benabdelouahab, Y.; Muñoz-Moreno, L.; Frik, M.; de la Cueva-Alique, I.; El Amrani, M.A.; Contel, M.; Bajo, A.M.; Cuenca, T.; Royo, E. Hydrogen bonding and anticancer properties of water-soluble chiral *p*-cymene Ru(II) compounds with amino-oxime ligands. *Eur. J. Inorg. Chem.* **2015**, *2015*, 2295–2307. [[CrossRef](#)]
38. de la Cueva-Alique, I.; Muñoz-Moreno, L.; Benabdelouahab, Y.; Elie, B.T.; El Amrani, M.A.; Mosquera, M.E.; Contel, M.; Bajo, A.M.; Cuenca, T.; Royo, E. Novel enantiopure cyclopentadienyl Ti(IV) oximato compounds as potential anticancer agents. *J. Inorg. Biochem.* **2016**, *156*, 22–34. [[CrossRef](#)]
39. de la Cueva-Alique, I.; Sierra, S.; Pérez-Redondo, A.; Marzo, I.; Gude, L.; Cuenca, T.; Royo, E. Study of the anticancer properties of optically active titanocene oximato compounds. *J. Organomet. Chem.* **2019**, *881*, 150–158. [[CrossRef](#)]
40. de la Cueva-Alique, I.; de la Torre-Rubio, E.; Muñoz-Moreno, L.; Calvo-Jareño, A.; Perez-Redondo, A.; Gude, L.; Cuenca, T.; Royo, E. Stereoselective synthesis of oxime containing Pd(II) compounds: Highly effective, selective and stereoregulated cytotoxicity against carcinogenic PC-3 cells. *Dalton Trans.* **2022**, *51*, 12812–14828. [[CrossRef](#)]
41. de la Cueva-Alique, I.; Muñoz-Moreno, L.; de la Torre-Rubio, E.; Bajo, A.M.; Gude, L.; Cuenca, T.; Royo, E. Water soluble, optically active monofunctional Pd(II) and Pt(II) compounds: Promising adhesive and antimigratory effects on human prostate PC-3 cancer cells. *Dalton Trans.* **2019**, *48*, 14279–14293. [[CrossRef](#)]
42. Kukushkin, V.Y.; Pombeiro, A.J.L. Oxime and oximate metal complexes: Unconventional synthesis and reactivity. *Coord. Chem. Rev.* **1999**, *181*, 147–175. [[CrossRef](#)]
43. Motaleb, M.A.; Selim, A.A. Dioximes: Synthesis and biomedical applications. *Bioorg. Chem.* **2019**, *82*, 145–155. [[CrossRef](#)] [[PubMed](#)]
44. Schepetkin, I.A.; Plotnikov, M.B.; Khlebnikov, A.I.; Plotnikova, T.M.; Quinn, M.T. Oximes: Novel therapeutics with anticancer and anti-inflammatory potential. *Biomolecules* **2021**, *11*, 777. [[CrossRef](#)] [[PubMed](#)]
45. Brecknell, D.J.; Carman, R.M.; Singaram, B.; Verghese, J. Silvestrene nitrosochlorides and derived amino-oximes. *Aust. J. Chem.* **1977**, *30*, 195–203. [[CrossRef](#)]
46. Faller, J.W.; Patel, B.P.; Albrizzio, M.A.; Curtis, M. Diastereoselectivity in chiral ruthenium complexes of bidentate bisphosphine monoxide ligands: controlling epimerization in aldehyde complexes and 16-electron intermediates. *Organometallics* **1999**, *18*, 3096–3104. [[CrossRef](#)]
47. Faller, J.W.; Sarantopoulos, N. Novel binding modes and hemilability in atropisomeric phosphino–amino palladium complexes. *Organometallics* **2004**, *23*, 2008–2014. [[CrossRef](#)]
48. Bigotto, A.; Costa, G.; Galasso, V.; De Altı, G. Infra-red spectra and normal vibrations of bis-dimethylglyoximates of transition metals. *Spectrochim. Acta A* **1970**, *26*, 1939–1949. [[CrossRef](#)]
49. Thorton, D.A. Metal complexes of aniline: Infrared and raman spectra. *J. Coord. Chem.* **1991**, *24*, 261–289. [[CrossRef](#)]
50. Nakamoto, K. Halogeno Complexes. In *Infrared and Raman Spectra of Inorganic and Coordination Compounds—Part B: Applications in Coordination, Organometallic and Bioinorganic Chemistry*, 6th ed.; John Wiley & Sons: Hoboken, NJ, USA, 2009; pp. 193–196.
51. Bandyopadhyay, N.; Zhu, M.; Lu, L.; Mitra, D.; Das, M.; Das, P.; Samanta, A.; Naskar, J.P. Synthesis, structure, spectral characterization, electrochemistry and evaluation of antibacterial potentiality of a novel oxime-based palladium(II) compound. *Eur. J. Med. Chem.* **2015**, *89*, 59–66. [[CrossRef](#)]
52. Salih, B.M.M.; Satyanarayana, S. Vitamin B<sub>12</sub> models: Synthesis and characterization of cyano bridged dicobaloximes and antimicrobial activity. *Afr. J. Pure Appl. Chem.* **2009**, *3*, 170–176.
53. Lippolis, V.; Blake, A.J.; Cooke, P.A.; Isaia, F.; Li, W.-S.; Schröder, M. Synthesis and full characterisation of the first discrete binuclear complex featuring a two-electron ( $\sigma$ )  $\mu_2$ - $\kappa$ C: $\kappa$ C bridging cyanide. *Chem. Eur. J.* **1999**, *5*, 1987–1991. [[CrossRef](#)]
54. Laidlaw, W.M.; Denning, R.G. Synthesis and characterisation of cyanide-bridged heterobinuclear mixed-valence compounds based on cyclopentadienylorganophosphine-ruthenium(II) and -osmium(II) cyano and pentaammine-ruthenium(III) and -osmium(III) moieties. *J. Chem. Soc. Dalton Trans.* **1994**, 1987–1994. [[CrossRef](#)]
55. Kettle, S.F.A.; Aschero, G.L.; Diana, E.; Rossetti, R.; Stanghellini, P.L. The vibrational spectra of the cyanide ligand revisited: terminal cyanides. *Inorg. Chem.* **2006**, *45*, 4928–4937. [[CrossRef](#)] [[PubMed](#)]
56. Nakamoto, K. Cyano and Nitrile Complexes. In *Infrared and Raman Spectra of Inorganic and Coordination Compounds—Part B: Applications in Coordination, Organometallic and Bioinorganic Chemistry*, 6th ed.; John Wiley & Sons: Hoboken, NJ, USA, 2009; pp. 116–117.
57. Karadag, A.; Pasaoglu, H.; Kastas, G.; Büyükgüngör, O. Synthesis, IR spectrum, thermal behaviour and crystal structure of a novel one-dimensional cyano-bridged zinc(II)/nickel(II) complex. *Z. Kristallogr. Cryst. Mater.* **2005**, *220*, 74–78. [[CrossRef](#)]
58. Hanusa, T.P. Cyanide complexes of the transition metals. In *Encyclopedia of Inorganic Chemistry*, 2nd ed.; King, R.B., Crabtree, R.H., Lukehart, C.M., Atwood, D.A., Scott, R.A., Eds.; John Wiley & Sons: Chichester, UK, 2006. [[CrossRef](#)]
59. Nakamoto, K. *Infrared and Raman Spectra of Inorganic and Coordination Compounds—Part A: Theory and Applications in Inorganic Chemistry*, 6th ed.; John Wiley & Sons: Hoboken, NJ, USA, 2009; pp. 180–184.

60. v. Ahsen, B.; Bley, B.; Proemmel, S.; Wartchow, R.; Willner, H.; Aubke, F. Synthesen und schwingungsspektren der homoleptischen acetonitrilkomplex-kationen  $[\text{Au}(\text{NCCH}_3)_2]^+$ ,  $[\text{Pd}(\text{NCCH}_3)_4]^{2+}$ ,  $[\text{Pt}(\text{NCCH}_3)_4]^{2+}$  und des adduktes  $\text{CH}_3\text{CN}\cdot\text{SbF}_5$ . Kristallstrukturen der salze  $[\text{M}(\text{NCCH}_3)_4][\text{SbF}_6]_2\cdot\text{CH}_3\text{CN}$ , M = Pd, Pt. *Z. Anorg. Allg. Chem.* **1998**, *624*, 1225–1234. [CrossRef]
61. Tsiminis, G.; Schartner, E.P.; Brooks, J.L.; Hutchinson, M.R. Measuring and tracking vitamin B<sub>12</sub>: A review of current methods with a focus on optical spectroscopy. *Appl. Spectrosc. Rev.* **2017**, *52*, 439–455. [CrossRef]
62. Bao-Sheng, L.; Jing, G.; Geng-Liang, Y. Determination of vitamin B<sub>12</sub> concentration by fluorescence quenching with Acridine Orange-Rhodamine 6G energy transfer system. *Spectr. Spectral Anal.* **2005**, *25*, 1080–1082.
63. Shang, Z.B.; Wen, Y.J.; Yan, X.Q.; Sun, H.H.; Wang, Y.; Jin, W.J. Synthesis of a novel fluorescent probe based on 7-nitrobenzo-2-oxa-1,3-diazole skeleton for the rapid determination of vitamin B<sub>12</sub> in pharmaceuticals. *Luminescence* **2014**, *29*, 598–602. [CrossRef]
64. Song, P.-S. Spectroscopic analysis of vitamin B<sub>12</sub> derivatives. *Meth. Enzymol.* **1980**, *678*, 5–11.
65. Lodowski, P.; Toda, M.J.; Ciura, K.; Jaworska, M.; Kozlowski, P.M. Photolytic properties of Antivitamins B<sub>12</sub>. *Inorg. Chem.* **2018**, *57*, 7838–7850. [CrossRef]
66. Jones, A.R. The photochemistry and photobiology of vitamin B<sub>12</sub>. *Photochem. Photobiol. Sci.* **2017**, *16*, 820–834. [CrossRef]
67. Lawrence, A.D.; Nemoto-Smith, E.; Deery, E.; Baker, J.A.; Schroeder, S.; Brown, D.G.; Tullet, J.M.A.; Howard, M.J.; Brown, I.R.; Smith, A.G.; et al. Construction of fluorescent analogs to follow the uptake and distribution of cobalamin (vitamin B<sub>12</sub>) in bacteria, worms, and plants. *Cell Chem. Biol.* **2018**, *25*, 941–951. [CrossRef]
68. Sugiarto, T.; Isnaeni, I.; Putri, K.J. Analysis of dual peak emission from Rhodamine 6G organic dyes using photoluminescence. *J. Phys. Conf. Ser.* **2017**, *817*, 012047. [CrossRef]
69. Mahasin, F.; Al-Kadhemy, H.; Abbas, K.N.; Abdalmuhdi, W.B. Physical properties of Rhodamine 6G laser dye combined in polyvinyl alcohol films as heat sensor. *IOP Conf. Ser. Mater. Sci. Eng.* **2020**, *928*, 072126.
70. Karolin, J.; Bogen, S.T.; Johansson, L.B. Å. Polarized fluorescence and absorption spectroscopy of 1,32-dihydroxy-dotriacontane-bis-rhodamine 101 ester. A new and lipid bilayer-spanning probe. *J. Fluoresc.* **1995**, *5*, 279–284. [CrossRef]
71. Geoghegan, K.F.; Emery, M.J.; Martin, W.H.; McColl, A.S.; Daumy, G.O. Site-directed double fluorescent tagging of human renin and collagenase (MMP-1) substrate peptides using the periodate oxidation of N-terminal serine. An apparently general strategy for provision of energy-transfer substrates for proteases. *Bioconjug. Chem.* **1993**, *4*, 537–544. [CrossRef] [PubMed]
72. Rajasekar, M. Recent Trends in Rhodamine derivatives as fluorescent probes for biomaterial applications. *J. Mol. Struct.* **2021**, *1235*, 130232. [CrossRef]
73. Tian, M.; Peng, X.; Fan, J.; Wang, J.; Sun, S. A fluorescent sensor for pH based on rhodamine fluorophore. *Dye. Pigment.* **2012**, *95*, 112–115. [CrossRef]
74. Zehentbauer, F.M.; Moretto, C.; Stephen, R.; Thevar, T.; Gilchrist, J.R.; Pokrajac, D.; Richard, K.L.; Kiefer, J. Fluorescence spectroscopy of Rhodamine 6G: Concentration and solvent effects. *Spectrochim. Acta A* **2014**, *121*, 147–151. [CrossRef] [PubMed]
75. Beija, M.; Afonso, C.A.; Martinho, J.M. Synthesis and applications of Rhodamine derivatives as fluorescent probes. *Chem. Soc. Rev.* **2009**, *38*, 2410–2433. [CrossRef] [PubMed]
76. Liu, X.; Testa, B.; Fahr, A. Lipophilicity and its relationship with passive drug permeation. *Pharm. Res.* **2011**, *28*, 962–977. [CrossRef] [PubMed]
77. Lipinski, C.A.; Lombardo, F.; Dominy, B.W.; Feeney, P.J. Experimental and computational approaches to estimate solubility and permeability in drug discovery and development settings. *Adv. Drug Deliv. Rev.* **2001**, *46*, 3–26. [CrossRef] [PubMed]
78. Andrés, A.; Rosés, M.; Ràfols, C.; Bosch, E.; Espinosa, S.; Segarra, V.; Huerta, J.M. Setup and validation of shake-flask procedures for the determination of partition coefficients ( $\log D$ ) from low drug amounts. *Eur. J. Pharm. Sci.* **2015**, *76*, 181–191. [CrossRef] [PubMed]
79. Rossier, J.; Delasoie, J.; Haeni, L.; Hauser, D.; Rothen-Rutishauser, B.; Zobi, F. Cytotoxicity of Mn-based photoCORMs of ethynyl- $\alpha$ -diimine ligands against different cancer cell lines: The key role of CO-depleted metal fragments. *J. Inorg. Biochem.* **2020**, *209*, 111122. [CrossRef] [PubMed]
80. Takahashi, K.; Tavassoli, M.; Jacobsen, D.W. Receptor binding and internalization of immobilized transcobalamin II by mouse leukaemia cells. *Nature* **1980**, *288*, 713–715. [CrossRef] [PubMed]
81. Kutushov, M.; Gorelik, O. Low concentrations of Rhodamine-6G selectively destroy tumor cells and improve survival of melanoma transplanted mice. *Neoplasma* **2013**, *60*, 262–273. [CrossRef] [PubMed]
82. Magut, P.K.S.; Das, S.; Fernand, V.E.; Losso, J.; McDonough, K.; Naylor, B.M.; Aggarwal, S.; Warner, I.M. Tunable cytotoxicity of rhodamine 6G via anion variations. *J. Am. Chem. Soc.* **2013**, *135*, 15873–15879. [CrossRef]
83. Cooper, G.M. *The Cell: A Molecular Approach*, 2nd ed.; Sinauer Associates: Sunderland, MA, USA, 2000. Available online: <https://www.ncbi.nlm.nih.gov/books/NBK9847/> (accessed on 15 March 2024).
84. Stewart, Z.A.; Westfall, M.D.; Pietenpol, J.A. Cell-cycle dysregulation and anticancer therapy. *Trends Pharmacol. Sci.* **2003**, *24*, 139–145. [CrossRef]
85. Jäckel, M.; Köpf-Maier, P. Influence of cisplatin on cell-cycle progression in xenografted human head and neck carcinomas. *Cancer Chemother. Pharmacol.* **1991**, *27*, 464–471. [CrossRef]
86. Gear, A.R. Rhodamine 6G. A potent inhibitor of mitochondrial oxidative phosphorylation. *J. Biol. Chem.* **1974**, *249*, 3628–3637. [CrossRef]

87. Jung, Y.; Lippard, S.J. Direct cellular responses to platinum-induced DNA damage. *Chem. Rev.* **2007**, *107*, 1387–1407. [[CrossRef](#)] [[PubMed](#)]
88. Chaires, J.B. Structural selectivity of drug-nucleic acid interactions probed by competition dialysis. In *Topics in Current Chemistry—DNA Binders and Related Subjects*; Waring, M.J., Chaires, J.B., Eds.; Springer: Berlin-Heidelberg, Germany, 2005; Volume 253, pp. 33–53.
89. Oxford Diffraction. *CrysAlis CCD*; Oxford Diffraction Ltd.: Abingdon, UK, 2006.
90. Sheldrick, G.M. SHELXT—Integrated space-group and crystal-structure determination. *Acta Cryst.* **2015**, *A71*, 3–8. [[CrossRef](#)] [[PubMed](#)]
91. Sheldrick, G.M. Crystal structure refinement with SHELXL. *Acta Cryst.* **2015**, *C71*, 3–8.
92. McArdle, P.; Gilligan, K.; Cunningham, D.; Dark, R.; Mahon, M. A method for the prediction of the crystal structure of ionic organic compounds—The crystal structures of *o*-toluidinium chloride and bromide and polymorphism of bicifadine hydrochloride. *CrystEngComm* **2004**, *6*, 303–309. [[CrossRef](#)]
93. Farrugia, L.J. WinGX and ORTEP for Windows: An update. *J. Appl. Crystallogr.* **2012**, *45*, 849–854. [[CrossRef](#)]
94. Taraszka, K.S.; Chen, E.; Metzger, T.; Chance, M.R. Identification of structural markers for vitamin B<sub>12</sub> and other corrinoid derivatives in solution using FTIR spectroscopy. *Biochemistry* **1991**, *30*, 1222–1227. [[CrossRef](#)]
95. Zhou, K.; Zelder, F. Vitamin B<sub>12</sub> mimics having a peptide backbone and tuneable coordination and redox properties. *Angew. Chem. Int. Ed.* **2010**, *49*, 5178–5180. [[CrossRef](#)] [[PubMed](#)]
96. Calafat, A.M.; Marzilli, L.G. Investigations of B<sub>12</sub> derivatives with inorganic ligands using 2D NMR spectroscopy. Ligand-responsive shifts suggest that the deoxyadenosyl moiety in Coenzyme B<sub>12</sub> has a steric *trans* influence. *J. Am. Chem. Soc.* **1993**, *115*, 9182–9190. [[CrossRef](#)]
97. Horton, R.A.; Bagnato, J.D.; Grissom, C.B. Structural determination of 5'-OH alpha-ribofuranoside modified cobalamins via <sup>13</sup>C and DEPT NMR. *J. Org. Chem.* **2003**, *68*, 7108–7111. [[CrossRef](#)]
98. Brown, K.L.; Evans, D.R. Heteronuclear NMR studies of cobalt corrinoids. 14. Amide proton and nitrogen-15 NMR studies of base-on cobalamins. *Inorg. Chem.* **1993**, *32*, 2544–2548. [[CrossRef](#)]
99. Kurumaya, K.; Kajiwara, M. Proton nuclear magnetic resonance (<sup>1</sup>H-NMR) signal assignment of vitamin B<sub>12</sub> based on normal two-dimensional NMR and feeding experiments. *Chem. Pharm. Bull.* **1989**, *1*, 9–12. [[CrossRef](#)]
100. Ramos, S.S.; Vilhena, A.F.; Santos, L.; Almeida, P. <sup>1</sup>H and <sup>13</sup>C NMR spectra of commercial rhodamine ester derivatives. *Magn. Reson. Chem.* **2000**, *38*, 475–478. [[CrossRef](#)]
101. Akalin, E.; Akyüz, S. Force field and IR intensity calculations of aniline and transition metal(II) aniline complexes. *J. Mol. Struct.* **1999**, *482–483*, 175–181. [[CrossRef](#)]
102. Ibn El Alami, M.S.; El Amrani, M.A.; Dahdouh, A.; Roussel, P.; Suisse, I.; Mortreux, A.  $\alpha$ -Amino-oximes based on optically pure limonene: A new ligands family for ruthenium-catalyzed asymmetric transfer hydrogenation. *Chirality* **2012**, *24*, 675–682. [[CrossRef](#)]

**Disclaimer/Publisher's Note:** The statements, opinions and data contained in all publications are solely those of the individual author(s) and contributor(s) and not of MDPI and/or the editor(s). MDPI and/or the editor(s) disclaim responsibility for any injury to people or property resulting from any ideas, methods, instructions or products referred to in the content.